Clim. Past, 21, 857–876, 2025
https://doi.org/10.5194/cp-21-857-2025

Climate of the Past
Open Access
EGU

Subaqueous speleothems as archives of groundwater recharge on Australia's southern arid margin

Calla N. Gould-Whaley[1], Russell N. Drysdale[1], Pauline C. Treble[2,3], Jan-Hendrik May[1], Stacey C. Priestley[4], John C. Hellstrom[1], Christopher R. Vardanega[2], and Clare C. Buswell[5]

[1]School of Geography, Earth and Atmospheric Science, University of Melbourne, Parkville, 3010, Australia
[2]Environment Research Group, Australian Nuclear Science and Technology Organisation, Lucas Heights, 2234, Australia
[3]School of Biological, Earth and Environmental Sciences, University of New South Wales, Kensington, 2052, Australia
[4]Drought Resilience Mission, Commonwealth Scientific and Industrial Research Organisation, Adelaide, 5000, Australia
[5]College of Humanities, Arts and Social Sciences, Flinders University, Adelaide, 5001, Australia

Correspondence: Calla N. Gould-Whaley (cgould@student.unimelb.edu.au)

Received: 27 June 2024 – Discussion started: 22 July 2024
Revised: 2 December 2024 – Accepted: 11 December 2024 – Published: 7 May 2025

Abstract. As anthropogenic climate change enhances aridity across many regions of the globe, understanding drivers of aridification is more important than ever before. Unfortunately, arid regions globally tend to exhibit a paucity of palaeoclimate records, and the archives that are available typically comprise unconsolidated sediments prone to reworking, large dating uncertainties, and ambiguous climatic interpretations. This is certainly true of Australia's vast continental interior, which is dominated by harsh, arid conditions. Mairs Cave, in the southern Ikara-Flinders Ranges (South Australia), is located on the southern margin of the arid zone. In the present day, the cave is largely dry, and there is limited evidence of active speleothem growth. However, historical records and observations throughout the cave indicate that it was periodically flooded, suggesting the local water balance was once much more positive than it is today. The cave contains a curtain of hanging speleothems known as pendulites, which grow subaqueously when submerged in water that is saturated with respect to calcite. Geochemical evidence, including trace element concentrations, uranium isotope ratios, and dead carbon fractions (DCFs), indicates that a rise in the local groundwater during periods of enhanced groundwater recharge is the cause of the cave flooding events that trigger pendulite growth. Uranium–thorium dating of a pendulite retrieved from Mairs Cave has revealed two multi-millennial growth phases (68.5–65.4 and 51.2–42.3 ka) and two short bursts of growth (18.9 and 16.4 ka) during the Last Glacial Period (LGP). The absence of subsequent pendulite growth suggests that strong water deficits under warm Holocene interglacial conditions give rise to episodic, rather than persistent, cave flooding.

1 Introduction

Spatial and temporal gaps in records of past climate limit our understanding of climate dynamics and variability, thus hindering the development of rigorous models that can predict the heterogenous manifestations and magnitudes of anthropogenic climate change (Skinner, 2008). Arid regions across the globe are underrepresented by palaeoclimate records when compared to humid regions due to environmental conditions that are not conducive to the capture or the preservation of palaeoclimate information (Falster et al., 2018; Fujioka and Chappell, 2010; Habeck-Fardy and Nanson, 2014). Moisture deficits preclude the existence of perennial lakes, bogs, and fens and limit the abundance of flora and fauna necessary to generate fossil records (Bateman et al., 2007; Carr et al., 2007; Field et al., 2018; Reeves et al., 2013b). Additionally, biological material tends to be poorly preserved in arid environments due to desiccation, photodegradation, oxidation, extreme temperature fluctuations, and physical weathering by abrasive sediments (Carr et al., 2007; Field et al., 2018; Fujioka and Chappell, 2010; Scott, 2016; Thomas and Burrough, 2016). Aeolian archives, while abundant in arid regions, can be difficult to interpret

given that modern analogues and mathematically modelled aeolian landscapes exhibit complex and non-linear responses to climate drivers (Fitzsimmons et al., 2013; Telfer et al., 2017).

Australia is no exception to the global pattern: the vast interior of the continent is dominated by harsh, dry conditions and is consequently lacking in palaeoclimate records when compared to the more humid coastal fringes (Reeves et al., 2013b). Given that Australia is the largest landmass in the Southern Hemisphere (SH), terrestrial records of Australian palaeoclimate are essential to understanding global climate change and variability. The higher density of records in coastal regions allows detailed, continuous, and well-dated reconstructions of past climate along the fringes of the continent (Cadd et al., 2021; Reeves et al., 2013a, b; Williams et al., 2009). However, these findings cannot be extrapolated to the arid interior. Kati Thanda / Lake Eyre, the ephemerally filled endorheic salt lake at the heart of the continent, has thus far been a focus of much palaeoclimate research in arid Australia (Cohen et al., 2022; DeVogel et al., 2004; Fu et al., 2017; Magee et al., 1995, 2004; May et al., 2022; Nanson et al., 1998). Beach ridges and other lacustrine landforms and sediments provide indisputable evidence of lake-filling events. However, the 1 200 000 km^2 catchment responsible for filling the lake sits largely to the north and receives rainfall from the Indo-Australian Summer Monsoon (IASM; Pook et al., 2014). Therefore, records of lake filling reflect hydroclimatic changes in the northern part of the continent rather than the climate of the interior itself.

Munda / Lake Frome is another endorheic salt lake 400 km SE of Kati Thanda. Inflow to Munda is primarily received as runoff from the Ikara-Flinders Ranges to the west, but lake filling can also occur if monsoonal rainfall in the northern reaches of the continent is especially high (May et al., 2015). Between Munda and Kati Thanda, there is a string of smaller lakes: Malakanha / Lake Callabonna, Lake Blanche, and Lake Gregory. During periods of especially high recharge, Munda, Malakanha, Blanche, and Gregory can overflow into one another and become a hydrologically connected mega-lake (mega-Munda; Cohen et al., 2012, 2015; May et al., 2015). There is also evidence to suggest that, during the most extreme pluvial periods of the LGP, mega-Munda and Kati Thanda became connected via overflow through the Warrawoocara Channel (Cohen et al., 2011, 2012; Leon and Cohen, 2012). While these lake systems provide indisputable evidence of large-scale environmental change, dating uncertainties still limit the utility of these sedimentary archives to detect climate events at millennial and centennial timescales through the Last Glacial Period (LGP) and beyond. As a result, our knowledge of the climatic past of Australia's arid interior remains fragmented both spatially and temporally.

Speleothems, secondary calcium carbonate deposits that form in caves, contain physical and chemical properties that can act as proxies of past climate change (Fairchild and Baker, 2012). Since speleothems are dateable by radiometric methods, the proxy records can be tethered to precise chronologies to produce climatic reconstructions with high temporal resolution, sub-annually in some cases (e.g. Faraji et al., 2024; Lu et al., 2021; Mattey et al., 2008; Van Rampelbergh et al., 2015). Speleothems with slower growth rates can provide exceedingly long, continuous records of past climate (e.g. Drysdale et al., 2020; Hodge et al., 2008; Ünal-Imer et al., 2016). Due to their subterranean setting, speleothems are largely shielded from surface processes capable of degrading, truncating, or eroding other terrestrial archives (Fairchild and Baker, 2012). While post-depositional alteration can occur, it is usually detectable, and affected specimens can be excluded from climate reconstructions (Bajo et al., 2016; Frisia, 2015; Martínez-Aguirre et al., 2019; Martín-García et al., 2014). Speleothems develop in carbonate bedrock terrains across the globe (Atsawawaranunt et al., 2018; Comas-Bru et al., 2020) and consequently have been employed to address a wide range of palaeoclimatic questions (e.g. Cheng et al., 2016; Corrick et al., 2020; Cruz et al., 2009; Dumitru et al., 2021; Vaks et al., 2013; Wang et al., 2008). Speleothems typically form when water drips from the cave ceiling, which means that (for at least part of the year) precipitation must exceed evapotranspiration such that water can infiltrate the subsurface (Fairchild and Baker, 2012). Therefore, encountering a speleothem-bearing cave in an environment that is now arid generally suggests that, at some point in the past, the local water balance was more positive. These speleothems can contain records of hydroclimate before and/or during the onset of aridification, which have never been more important than in our current era of anthropogenic climate change, which threatens enhanced aridity across many regions of the globe (Feng and Fu, 2013; Markowska et al., 2016, 2020).

Mairs Cave, in the central Ikara-Flinders Ranges, is situated at the southernmost tip of the Kati Thanda / Lake Eyre basin and on the boundary between the arid zone to the north and the semi-arid zone to the south (Fig. 1). The site is also at the interface between tropical and mid-latitudinal climate systems, receiving moisture from both the Southern Hemisphere westerly winds (SHWWs) and the IASM (Pook et al., 2014). Mairs Cave has been the subject of one previous palaeoclimate study (Treble et al., 2017), where regional palaeohydrology was reconstructed from two stalagmites that together spanned the Last Glacial Maximum (LGM) and early deglaciation. Stalagmites are the preferred speleothem type for past climate reconstructions, as they often exhibit thick and flat laminae along their central axis, which makes for easy sampling and high-resolution records (Fairchild and Baker, 2012). There are few stalagmites in Mairs Cave; to circumvent this issue, we chose to explore the potential of alternative formations as palaeoclimate archives.

Mairs Cave contains a curtain of pendulites. These unique formations begin as stalactites, then they become submerged in water that is supersaturated with respect to calcite, result-

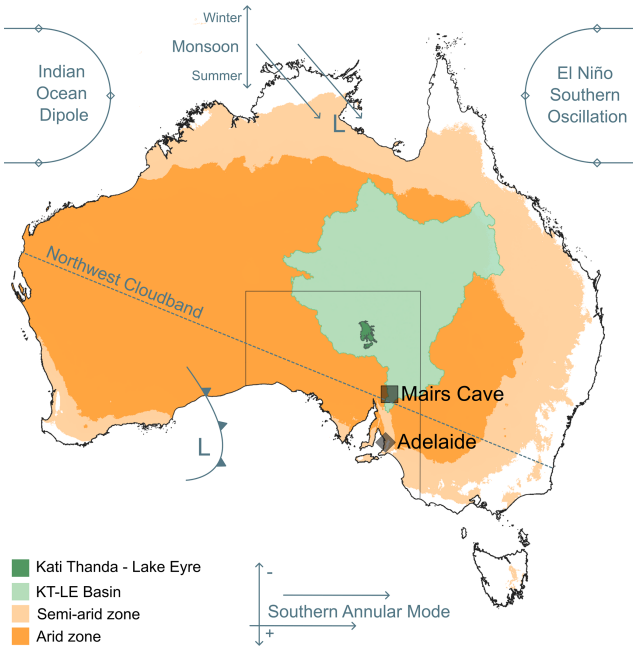

Figure 1. Location of Mairs Cave (study site) relative to Adelaide (the capital city of the state of South Australia). Location of Kati Thanda / Lake Eyre and the extent of the Kati Thanda / Lake Eyre basin. Regions designated arid are shown in dark orange ($0.05 < \mathrm{AI} < 0.2$), and regions designated semi-arid are shown in light orange ($0.2 < \mathrm{AI} < 0.5$; Trabucco and Zomer et al., 2022). Also depicted are the primary systems that influence climate at the study site. Colours were assigned according to recommendations of Crameri et al. (2020).

ing in subaqueous deposition of calcite on the existing stalactite surface (Field et al., 2002; Gillieson, 1996; Grimes, 2006; Jennings, 1979; Martini and Grimes, 2012). Hiatuses in subaqueous growth occur when water levels drop below the pendulite or when the water is no longer supersaturated with respect to calcium carbonate. In this study, we present morphological, microstratigraphic, and geochemical evidence to demonstrate that pendulite growth in Mairs Cave corresponds to intervals of higher local water table during periods of enhanced groundwater recharge. We conclude that these speleothems constitute important archives of past hydrological change in Australia's southern arid zone, where palaeoclimate records are lacking.

2 Site description

Mairs Cave (32.18° S, 138.87° E) is on Adnyamathanha Country in South Australia (Fig. 1). The site receives between 77.4 and 582.8 mm yr^{-1}, with a mean of 290.4 mm yr^{-1} (1917–2023; BoM, 2024a). Mean potential evapotranspiration is 1720 mm yr^{-1}, making the region one of extreme water deficit, with an aridity index of 0.17 (arid classification; Arora, 2002; Burrell et al., 2020; Zomer et al., 2022) and a Köppen–Geiger classification of BWk (cold desert; Beck et al., 2020). Winter rainfall is primarily delivered to the study site by low-pressure systems carried across the Southern Ocean by the SHWWs (Meneghini et al., 2007). Throughout the year, tropical moisture can be delivered to the region when moist air over the Indian Ocean moves poleward to create a Northwest Cloudband (NWCB) across Australia (Reid et al., 2020). Tropical moisture delivery can be enhanced during summer by southward propagation of depressions associated with the IASM (Dey et al., 2021; Pook et al., 2014; Reid et al., 2020). Positioned within reach of both tropical and mid-latitudinal climate systems, palaeoclimate archives from Mairs Cave thus have potential for tracking their influence on rainfall in southern Australia beyond the instrumental era.

Although there are many cave-bearing carbonate rock formations scattered across the Ikara-Flinders Ranges, the largest and most decorated caves, including Mairs, tend to occur in the Etina Formation (∼ 655 Ma), which is a sandy, oolitic, and stromatolitic limestone inter-bedded with siltstones (Fromhold and Wallace, 2012; Lawrence, 2009). Mairs Cave is situated in a strike ridge of Etina limestone that rises 16 m above the floodplain of Buckalowie Creek (Fig. 2a), an ephemeral waterway that runs parallel to the Etina outcrop in an NNE direction (Fig. 2b). Mairs Cave appears to have formed along the boundary between two distinct facies within the limestone, one easily weathered (the eastern wall) and the other less soluble (the western wall). The cave is accessed via a 17 m vertical shaft formed within the more weatherable facies. The base of the entrance shaft opens out to the main chamber of the cave (Fig. 2c), which is ∼ 100 m long and 12 m wide. Beyond the main chamber, the cave narrows and continues for an additional 120 m in a northeast direction, following the strike of the Etina limestone. Cave temperature measured by data loggers in 2019 ranges between 19.9 and 15.3 °C in the main chamber (open to the surface via the vertical entrance shaft), with a mean annual temperature of 18.0 °C. Temperatures are more stable in the interior of the cave, ranging between 21.8 and 21.4 °C, with an annual mean of 21.6 °C. Over the same period, daily surface air temperatures fluctuated between 44.6 and 6.7 °C, with a mean of 24.5 °C.

The western wall of the main chamber is near vertical and is thinly coated in calcite to a height of ∼ 3 m, suggestive of standing water (5 in Fig. 2d; Fig. 3a). Large breakdown blocks fallen from the cave ceiling are coated with thin layers of calcite (4 in Fig. 2d; Fig. 3b and c). The eastern wall is well decorated with an assemblage of pendulites, exhibiting the bulbous, cauliflower-like surface morphology indicative of a subaqueous growth setting (2 in Fig. 2c and d; Fig. 3e). Throughout the cave, the floor and lower shelves are strewn with "calcite rafts", which are thin plates of calcite that typically precipitate at the surface of a water body that is supersaturated with respect to calcium carbonate (Fig. 3d). Speleothem rubble is scattered throughout the cave but is

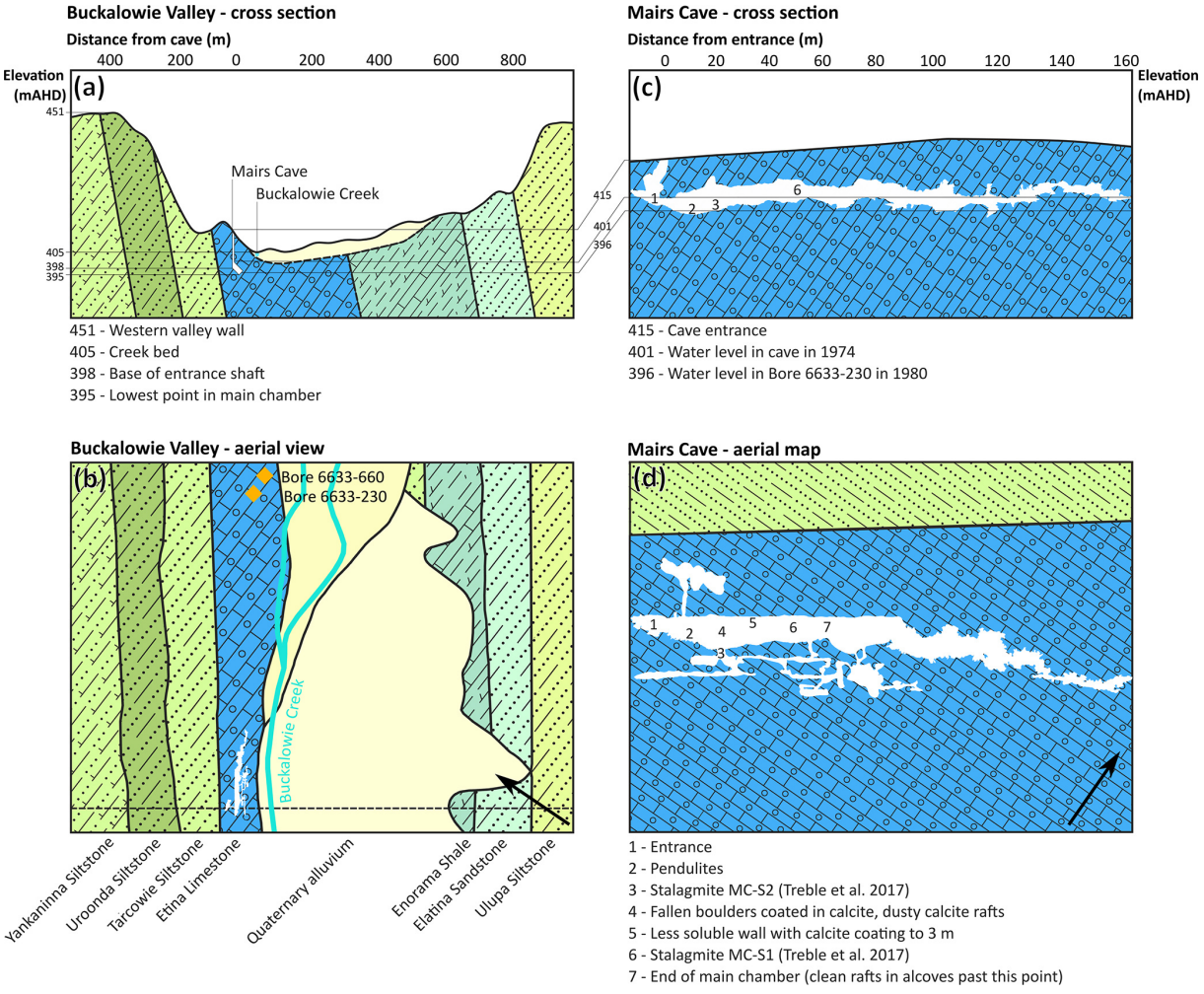

Figure 2. **(a)** Cross-section of Buckalowie Valley indicating the positions of Mairs Cave and Buckalowie Creek and the elevations of the relevant features referred to in the text. **(b)** Aerial view of Buckalowie Valley showing the geological formations present. The dashed line indicates the position of the cross-section in panel **(a)**. The distance from the cave entrance can be read in panel **(a)**. **(c)** Cross-section of Mairs Cave showing the elevations of the relevant features referred to in the text (extracted from a 3D model of the cave). **(d)** Aerial map of the cave (extracted from a 3D model of the cave, cross-checked against the original map published by the Cave Exploration Group of South Australia, with surveying and mapping carried out by Sexton et al., 1958). The distance from the cave entrance can be read in panel **(c)**. mAHD is elevation in metres with respect to the Australian Height Datum.

mostly cemented to the cave floor by calcite coatings. Collectively, these observations indicate that, despite the present arid conditions, the chamber was once at least partially filled with water supersaturated with respect to calcite. Stalagmites MC-S1 and MC-S2 studied by Treble et al. (2017) were retrieved from the main chamber (6 in Fig. 2c and d) and from a side passage off the main chamber (3 in Fig. 2c and d). MC-S2 contains layers of calcified sediment, most likely deposited when floodwater mobilised sediments on the cave floor. MC-S1 exhibits no visible sediment layers, presumably because it sat higher in the cave and on top of a boulder, meaning it was not within reach of the sediment on the cave floor.

The cave is effectively dry today. Some formations appear damp but not actively dripping, precluding a dripwater monitoring study. Reports in the South Australian Department of Mines Annual Review noted that guano mining efforts in the cave had been hindered by a deep pool of standing water in the main chamber (Winton, 1920, 1922). In the archived newsletters of the Cave Exploration Group of South Australia (1956–present, available from the Australian Speleological Society at https://st1.asflib.net/JNS/SA/CEGSA/CEGSA-Pubs.html, last access: 26 June 2024), three trip reports mention the presence of standing water in Mairs Cave. Since cave flooding is a noteworthy event, we assume there was no water within the cave if no mention of water is made in a trip report. Flooding of the cave was ob-

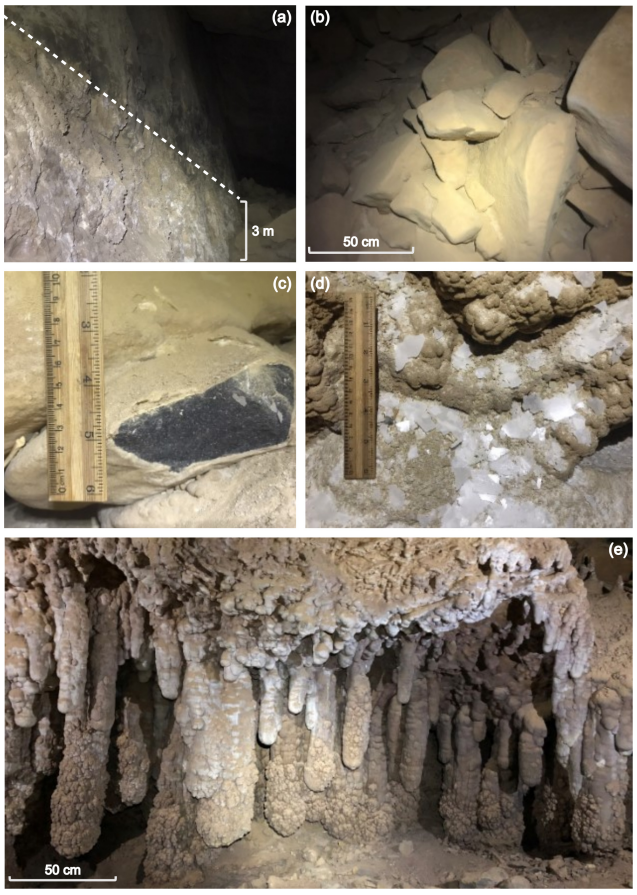

Figure 3. Photos taken in Mairs Cave. **(a)** Calcite precipitated on the western wall of the main chamber to a height of 3 m. **(b)** Breakdown blocks in the main chamber. **(c)** Small breakdown block in the main chamber that has been cleft to display calcite overgrowth. **(d)** Calcite rafts in an alcove along the passage past the main chamber. **(e)** Curtain of pendulites suspended from the ceiling of an overhang on the eastern wall of the main chamber.

served in June of 1968. A trip report from 3 months prior made no mention of water in the cave. In June 1974, there was approximately 3 m of water in the bottom of the shaft. Cave divers noted that the water was "crystal clear". A trip in December of the same year reported water at the base of the entrance shaft 15 cm deep. In addition to these three trips where water was observed within the cave, 44 trip reports either noted the absence of water or made no mention of water.

Despite near-total dependence on groundwater resources, the hydrogeology of the Ikara-Flinders Ranges has not been extensively studied (Fildes et al., 2020; Harrington and Cook, 2014). No hydrogeological studies have taken place in Buckalowie Valley, but findings from elsewhere in the region suggest that ridges of resistant formations tend to create hydrological divides between aquifers hosted in more fractured and/or porous formations (Ahmed et al., 2021; Ahmed and Clark, 2016; Fildes et al., 2020). Buckalowie Valley is constrained on either side by siltstone aquitards with extremely low primary porosity (Yankaninna, Uroonda, Tarcowie, and Ulupa siltstones in Fig. 2a and b); therefore it is likely that the boundaries of the aquifer roughly align with the topographic boundaries of the valley. There are only five bores within the valley, for which there are limited data available and no long-term monitoring. The lack of data precludes potentiometric surface mapping or hydrogeological modelling to establish the flow direction, recharge/discharge areas, or aquifer volume. In 1980, a bore (unit number 6633-230; Fig. 2b) was drilled into the Etina limestone 0.9 km NNE of the cave entrance. The standing water level at the time was 5.54 m below the surface (Fig. 2a). In 2018, the original bore was sealed, and a new bore (unit number 6633-660; Fig. 2b) was drilled 50 m to the east to facilitate transition to a solar-powered pump. Given the proximity of the bore, the age of the Etina limestone (> 635 Ma; Giddings et al., 2009) and the hydrological connectivity generally observed in mature karst landscapes (Ford and Williams, 2013; LeGrand, 1983; LeGrand and Stringfield, 1971), it is quite likely that the aquifer from which the bore draws water is continuous along the entire length of the limestone outcrop.

3 Methods and materials

3.1 Pendulite sampling and analyses

We collected a small pendulite (MC19; 4×10 cm) from a discrete position behind a curtain of larger pendulites, ensuring its removal was neither visible nor damaging to surrounding formations. The specimen was halved using a diamond masonry blade, set in epoxy resin for sampling, and polished to reveal the internal stratigraphy. To identify changes in the calcite fabric, a thin section was prepared for petrographic examination, which was carried out using a Leica DM750 polarising microscope. For uranium–thorium dating, powders of approximately 10 mg were milled from laminae before and after suspected hiatuses, using a New Wave MicroMill. Uranium–thorium (U–Th) measurements were taken on a Nu Plasma multicollector inductively coupled plasma mass spectrometer (MC-ICP-MS) in the Isotope Geochemistry Laboratory at the University of Melbourne using the protocols of Hellstrom (2003, 2006). Ages were corrected with an initial thorium (^{230}Th/^{232}Th) activity ratio of 1.5 ± 1.5.

Cation concentrations (Mg, Ca, Sr) in MC19 and NIST-610 glass were measured using a HelEx laser ablation system with a Lambda Physik COMPex 110 ArF excimer laser (193 nm) coupled to an Agilent 7700× quadrupole ICP-MS (Drysdale et al., 2012; Jochum et al., 2011). The 8.5 mm long scan line crossed the boundary from the internal stalactite to the suspected subaqueous material, with a pre-ablation spot size of 60 µm and a data collection spot size of 26 µm. Pre-ablation was performed with a laser pulse rate of 15 Hz, which was reduced to 10 Hz for data collection. Scan velocity was set to 13 µm s^{-1}, and laser fluence was set to 3 J cm^{-2}.

3.2 Calcite raft sampling and analyses

Calcite rafts on the floor of the main chamber were covered in a layer of fine sediment. A single dusty raft (MCCR-33) was collected. About 10 mg of the dusty exterior was removed with a scalpel and reserved for U–Th isotopic analysis (MCCR-33_1). From the exposed surface, another 10 mg was removed (MCCR-33_2), followed by another 10 mg (MCCR-33_3) until visibly clean calcite remained, from which a final 10 mg was sampled (MCCR-33_4). These four samples with decreasing degrees of dust contamination underwent U–Th isotopic analysis to better constrain the initial thorium required for correcting the U–Th ages of the calcite rafts. U–Th analysis of the calcite raft samples occurred according to the same procedure as analysis of the pendulite samples.

Rafts on ledges and in hollows along the cave wall were generally cleaner and thicker and exhibited larger crystals. Four clean calcite rafts (MCCR-25, 26, 30, 31) were collected for paired U–Th and radiocarbon analysis. From each raft, a chip (15 mg) underwent U–Th isotopic analysis. The remainder of each sample was reacted with 85 % H_3PO_4 at room temperature. CO_2 evolved from the outer portion of each sample (ca. 12 % by weight) was pumped away to avoid sample surface contamination with atmospheric CO_2. The sample was then transferred to a hot block at 90°, and the CO_2 that evolved over a 1 h period was converted to graphite using the Fe/H_2 method (Hua et al., 2001). Accelerator mass spectrometry (AMS) ^{14}C measurement was carried out using the Australian Nuclear Science and Technology Organisation (ANSTO) VEGA accelerator (Wilcken et al., 2015). After correction for machine background, procedural blank, and isotopic fractionation using measured $\delta^{13}C$, ^{14}C content was reported as percent modern carbon (pMC) and radiocarbon age (Stuiver and Polach, 1977). The dead carbon fraction (DCF) was calculated for each of these samples according to Eq. (1) (Hua et al., 2012):

$$\mathrm{DCF} = \left(1 - \frac{A_{\mathrm{calcite}}}{A_{\mathrm{atm}}}\right) 100\,\%, \tag{1}$$

where A_{calcite} is the measured radiocarbon content of the calcite rafts (pMC) and A_{atm} is the radiocarbon content of the atmosphere (in pMC; from SHcal20, Hogg et al., 2020) at the time of calcite precipitation (established by U–Th dating).

An additional six clean calcite rafts (MCCR-10, 16, 18, 20, 22, 29) were collected from the cave, ground into fine powders, and homogenised. Subsamples of 0.5 mg were used for measuring cation concentrations. The remaining powder underwent U–Th dating. Mg / Ca and Sr / Ca ratios in the calcite rafts were determined by digesting 0.5 mg subsamples in 5 mL of a 3 % Supelco Suprapur HNO_3 solution. Measurements were carried out at ANSTO using a Thermo Fisher iCAP 7600 Duo inductively coupled plasma atomic emission spectrometer (ICP-AES) according to the procedure described by Carilli et al. (2014).

3.3 Groundwater sampling and analyses

Groundwater was sampled from the active bore closest to the cave (unit number 6633-660) in 2019, 2021, and 2022. The pump was left to purge for 30 min, equivalent to 3 times the volume of standing water within the bore. A Terumo 50 mL Luer lock syringe was rinsed three times with bore water, then a Millex filter unit with a 0.45 µm low-binding Millipore membrane was fitted to the syringe. The first 150 mL passing through the filter was discarded. HDPE collection bottles (acid-washed prior to fieldwork) were rinsed with the filtrate three times before being filled to the brim and capped. Care was taken to leave no headspace in any of the bottles. After being firmly sealed, the lids and necks of the bottles were wrapped in Parafilm. A Supelco Suprapur 65 % HNO_3 spike was added to one of the blanks and to the bore water samples intended for major and minor cation analysis to reduce the pH to below 2. Upon returning to the laboratory, all samples were stored at 4 °C.

All groundwater analyses were performed at ANSTO. The concentrations of the major cations (Mg, Ca, and Sr) were measured on a Thermo Fisher iCAP 7600 ICP-AES. The concentration of U was measured using an Agilent 8900 triple quadrupole ICP-MS. Trace-element-to-calcium ratios ($X/\mathrm{Ca_{ppt}}$) in calcites that could theoretically precipitate from these groundwaters were calculated according to Eq. (2) using the measured groundwater ratios ($X/\mathrm{Ca_{soln}}$) and a range of partition coefficients (D_X) available in the literature (Day and Henderson, 2013; Drysdale et al., 2019; Fairchild et al., 2000; Huang et al., 2001; Huang and Fairchild, 2001; Tremaine and Froelich, 2013):

$$D_X = \frac{X/\mathrm{Ca_{ppt}}}{X/\mathrm{Ca_{soln}}}. \tag{2}$$

On the groundwater sample collected in 2022, the concentration of major anions (Cl^-, SO_4^{2-}, Br^-, and NO^{3-}) was measured using a Dionex ICS-2100 ion chromatograph. Saturation indices for calcite and other minerals were calculated using the WATEQ4F thermodynamic database in the program PHREEQC Interactive 3.7.3.15968 (Parkhurst and Appelo, 1999).

To constrain groundwater age, the tritium concentration was measured with a PerkinElmer Quantulus ultralow-level liquid scintillation analyser (LSA) following the procedures described by Morgenstern and Taylor (2009). Radiocarbon dating of the same water by AMS was performed according to the methods described in Wilcken et al. (2015). The radiocarbon age was rounded according to Stuiver and Polach (1977). The Han and Plummer closed-system model was used to correct the groundwater radiocarbon age to account for geochemical processes that occur along the flow path (Han and Plummer, 2013). The radiocarbon ages of groundwater were converted to calendar years before present (1950) using a calibration curve (Plummer and Glynn, 2013). For comparison to the calcite rafts, geochemical adjustment

models were used to estimate the DCF of the groundwater DIC, i.e. what portion of the carbon present in the groundwater sample was contributed by exchange with the bedrock or other "dead" carbon reservoirs (Han and Plummer, 2013; Kalin, 2000).

4 Results

4.1 Physical characteristics of MC19

The stratigraphy of MC19 can be macroscopically divided into two distinct facies. Inside the blue line in Fig. 4, the older, interior portion comprises white/grey calcite with regions of well-defined laminae, interspersed with blurry, poorly defined laminae and clear, featureless calcite. This internal portion exhibits both vertical and horizontal extension. In conjunction with the fact that calcite growth is emanating from the upper section that was attached to the cave ceiling, these features clearly indicate this portion of MC19 is a composite stalactite exposed in long section. Outside of the blue line in Fig. 4, the exterior growth is beige/brown in colour and clearly laminated throughout with a distinctive radial growth pattern. This composite structure is typical of a pendulite, a speleothem that begins as a stalactite in an air-filled cave and becomes submerged in a body of water that is supersaturated with respect to calcite, at which point the original stalactite acts as a nucleus upon which calcite is subaqueously deposited for as long as the pendulite remains submerged and the water remains supersaturated with respect to calcite (Field et al., 2002; Gillieson, 1996; Grimes, 2006; Jennings, 1979; Martini and Grimes, 2012).

The transition from the stalactite to the subaqueous material can also be identified in thin section (see Fig. 5a). Flat stalactite laminae are crosscut by thick, rounded, micritic layers. This angular unconformity suggests a dissolution event (e.g. via condensation corrosion) occurred prior to the subaqueous deposition of calcite. The subaqueous material is primarily composed of composite crystals interrupted by layers of clotted peloidal micrite (M in Fig. 5b) and microsparite (Ms in Fig. 5b). We interpret the thickest and darkest micritic layers as corresponding to extended growth hiatuses and stretches free of micrite correspond to periods of uninterrupted growth, i.e. sustained flooding of the cave. By extension, clustered yet distinct micrite layers may be indicative of fitful growth due to intermittent cave flooding.

4.2 Trace elements

Trace element concentrations in MC19 were measured along a transect that traversed the boundary between the internal stalactite and the subaqueous overgrowth (brown line in Fig. 4). There were abrupt increases in all trace elements when crossing into the subaqueously deposited calcite. For example, mean Mg / Ca values increased from 7.70 mmol mol^{-1} in the stalactite to 36.25 mmol mol^{-1} in the subaqueous material. Mean Sr / Ca increased from 0.30–0.71 mmol mol^{-1}. In the calcite rafts, average Mg / Ca was 38.00 mmol mol^{-1} and average Sr / Ca was 0.87 mmol mol^{-1}. Groundwater cation concentrations measured in samples collected in 2019, 2021, and 2022 are shown in Table 1. Mg / Ca was 0.93, 1.02, and 1.00 mol mol^{-1} in the 3 years respectively. Sr / Ca was 5.42, 5.63, and 5.77 mmol mol^{-1}.

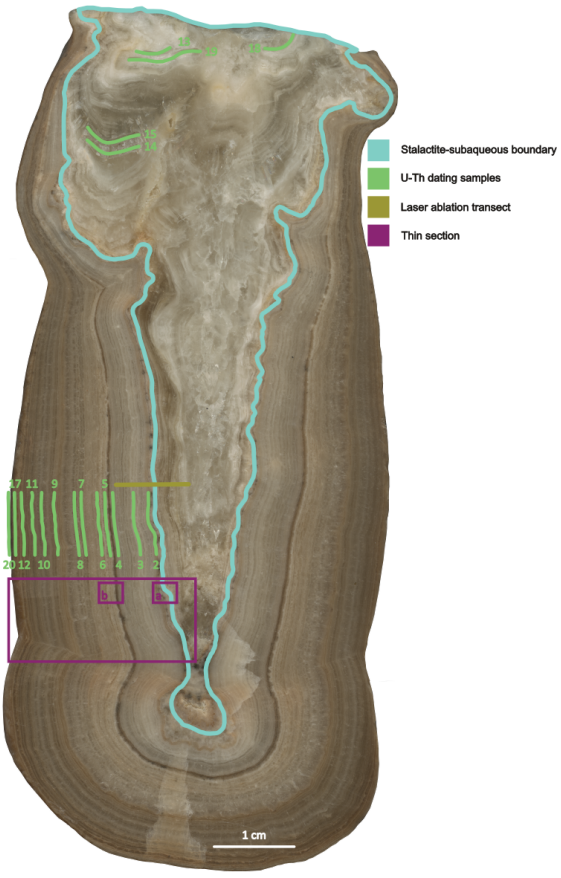

Figure 4. MC19 in vertical cross-section, with the boundary between the internal stalactite and the external subaqueous material indicated by the blue line. The laser ablation transect is indicated by the brown line. The U–Th sampling positions are indicated by the green lines. The area from which the thin section was taken is marked in purple. The two smaller purple boxes correspond to the thin-section images in Fig. 5a and b. Colours are assigned according to the recommendations of Crameri et al. (2020).

In Fig. 6, the range of trace-element-to-calcium ratios that could occur in calcite precipitated from the measured groundwater are presented (shaded bands) alongside trace-element-to-calcium ratios observed in the speleothems (box and whisker plots). It is worth noting that only one set of partition coefficients was calculated from subaqueously precipitated calcite (Drysdale et al., 2019) and that none were calculated from calcite rafts (which precipitate on the surface of the water body, not at depth).

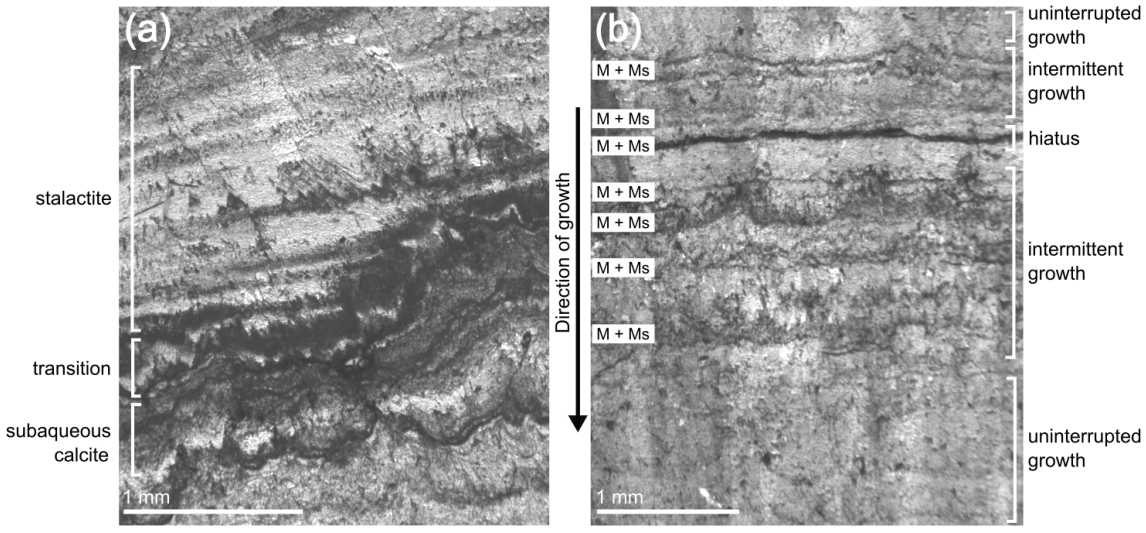

Figure 5. Thin-section images of MC19 under plane-polarised light. **(a)** At the transition between the stalactite and the subaqueous overgrowth. **(b)** The most visually prominent layer of micrite and microsparite in the subaqueous overgrowth. The area from which the thin section was taken is marked by the purple box in Fig. 4. The areas corresponding to the thin-section images in panels **(a)** and **(b)** are marked by the smaller purple boxes in Fig. 4.

Table 1. Cation concentrations measured in groundwater.

	Mg ($mmol\,L^{-1}$)	Sr ($\mu mol\,L^{-1}$)	Ca ($mmol\,L^{-1}$)
Groundwater sample 2019	4.40	25.56	4.72
Groundwater sample 2021	4.77	26.25	4.67
Groundwater sample 2022	4.69	27.05	4.61

Table 2. Physical properties and major anions measured on the groundwater sample collected in 2022.

Temperature (° C)	21.0
pH	8.11
Total alkalinity ($mg\,CaCO_3\,L^{-1}$)	294
Bicarbonate alkalinity ($mg\,CaCO_3\,L^{-1}$)	291
Carbonate alkalinity ($mg\,CaCO_3\,L^{-1}$)	3
Cl^- ($mg\,L^{-1}$)	940
SO_4^{2-} ($mg\,L^{-1}$)	262
Br^- ($mg\,L^{-1}$)	3.39
NO_3^- ($mg\,L^{-1}$)	10.7

4.3 Groundwater calcite saturation

Measurements of the groundwater sample taken in 2022 (Table 2) were used to calculate the calcite saturation index (1.12).

4.4 Speleothem age

The positions of the U–Th samples are indicated by green lines in Fig. 4. Two samples taken from the base of the embedded stalactite within the pendulite returned ages beyond the limits of uranium–thorium dating, with isotopic ratios indicating that the stalactite began growing more than 702 ka (MC19-18 and 13 in Table 3). Three other laminae within the stalactite returned ages of 513.0 (+85/ − 50), 258.1 (±4.6), and 250.0 (±4.7) ka (MC19-19, 15, and 14 in Table 3). The transition to subaqueous growth appears to have occurred around 68.5 (±0.40) ka (MC19-02 in Table 3) and continued until 65.4 (±0.49) ka (MC19-04 in Table 3). This growth period was followed by a 14 kyr hiatus, with subaqueous growth recommencing at 51.2 (±0.38) ka (MC19-05 in Table 3) and continuing through to 42.3 (±0.28) ka (MC19-12 in Table 3). A further brief burst of subaqueous growth occurred around 18.9 (±0.23) ka (MC19-17 in Table 3). A sample taken from the external growth lamina returned an age of 16.4 (±0.20) ka (MC19-20 in Table 3). Less than 1 mm of calcite was deposited during each of these last two periods of cave flooding. This is insufficient material for more than one dating sample, so the duration of these younger growth phases cannot be constrained. However, given the average growth rate during the two longer phases of subaqueous growth ($\sim 0.7\,mm\,kyr^{-1}$), the 1 mm of calcite deposited during each of these two brief bursts could correspond to ~ 1.4 kyr of growth. Initial uranium activity ratios

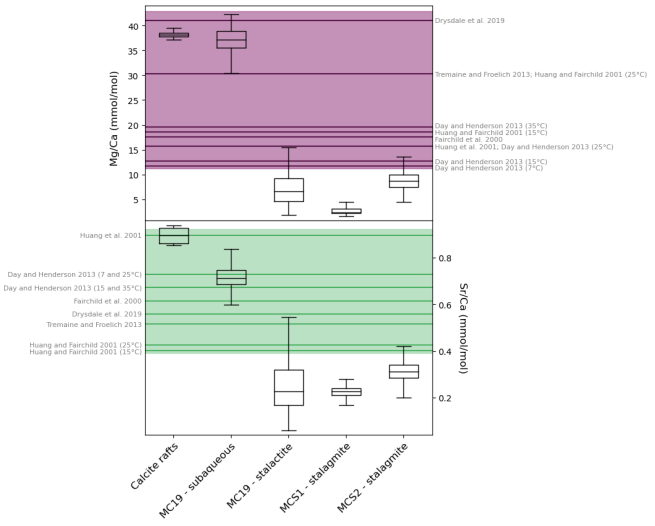

Figure 6. Upper-panel boxplots: Mg / Ca ratios in cave calcites. Lower-panel boxplots: Sr / Ca ratios in cave calcites. The bold purple lines (upper) and bold green lines (lower) indicate the X/Ca ratios that could occur in calcites precipitated from the groundwater. These values were calculated using the mean X/Ca ratios measured in the groundwater. The partition coefficients for each individual calculation are indicated in grey text. The purple (upper) and green (lower) shaded areas represent the full range of X/Ca ratios that could occur given the full range of X/Ca ratios measured in the groundwater. Colours are assigned according to the recommendations of Crameri et al. (2020).

($[^{234}\mathrm{U}/^{238}\mathrm{U}]_i$) are nearly 4 times lower in the stalactite samples than in those from the subaqueous material.

All calcite rafts returned ages within the last millennium. Rafts would have undoubtedly formed during older cave flooding events; however, their fragile nature would make long-term preservation unlikely, especially in light of recreational caving, archaeological excavation, and mining activities that have occurred since at least the 1920s. Samples from the dusty calcite raft (MCCR-33_1, 2, 3, and 4 in Table 3) produced ages of 1750, 1560, 1650, and 1710 CE, with ±2 s uncertainties of 1200, 260, 200, and 140 years respectively. Assuming coevality between subsamples, an initial thorium calculation was made ($[2.41 \pm 0.24]$) and the ages of all rafts corrected accordingly. Although the uncertainties decrease with decreasing dust contamination, all are substantially higher than the uncertainties on the ages of the clean rafts, which average ±8 years. One of the clean calcite rafts formed in 1073 (±18 yr) CE (MCCR-29 in Table 3), whilst the remaining clean rafts were dated to between 1879 and 1968 CE.

For the purpose of calculating the DCF, four rafts underwent paired U–Th and radiocarbon analyses. Two of the rafts (MCCR-25 and MCCR-30) formed during the post-bomb period (1965 and 1966 respectively), when atmospheric $^{14}\mathrm{C}$ was increasing rapidly. Given the uncertainties on the U–Th ages, atmospheric pMC at the time of raft formation cannot be accurately estimated, and these results were consequently discarded. The two rafts (MCCR-26 and MCCR-31) that formed in the pre-bomb period (1908 and 1940 respectively) returned DCFs of 41.38 (±0.31) and 40.45 (±0.33) % (Table 4).

4.5 Groundwater age

The radiocarbon results for the DIC in the groundwater (Table 5) returned a corrected age of 589 cal BP and a DCF of 45.8 % (Han and Plummer, 2013). The radiocarbon age can be considered the average age of the water within the sample. The presence of tritium (0.13 TU) is evidence that the aquifer also contains a portion of modern (post-1950) recharge (Clark, 2015).

5 Discussion

5.1 Mechanism of cave flooding

Together, the external morphology, internal stratigraphy, petrography, and trace element profiles of MC19 provide clear evidence for transition from classical stalactitic growth to subaqueous growth. The presence of calcite rafts, a standing water mark, and calcite overgrowths on boulders (see Fig. 3) and the evidence from historical documentation over the last 2 centuries provide further indication that Mairs Cave experiences periodic inundation. This raises the question of the mechanism by which the water enters the cave: invasion by runoff from overland flow, excessive vadose zone infiltration, or a rise in the regional groundwater table?

Buckalowie Creek is an ephemeral waterway that runs parallel to the strike of the Etina limestone formation and the long axis of the cave system (see Fig. 2a). The elevation of the modern creek bed is ∼ 10 m lower than the entrance to the cave but ∼ 10 m higher than the lowest point in the main chamber (Fig. 2a and c). It is unlikely that the creek could rise 10 m to flood the cave via the entrance shaft, given that floodwaters would need to occupy the broad width (400 m) of the floodplain before attaining the level of the entrance shaft. The creek has no nearby tributaries that could divert water into the cave. Similarly, there is no evidence on the land surface above the cave that would indicate flooding has occurred via the entrance shaft. In addition, flooding from overland flow would deliver water that is undersaturated with respect to calcite and would be unlikely to precipitate calcite even once chemical equilibrium was reached with the bedrock margins of the cave. Finally, overland flow would be highly turbid, but speleologists report clear water in the cave during the 1968 and 1974 inundation events. Thus, we eliminate direct invasion of overland flow as the dominant mechanism for cave flooding.

Standing water can be found in caves when periods of excessive dripwater discharge cause water to collect in depres-

https://doi.org/10.5194/cp-21-857-2025

Table 3. U–Th dating results for pendulite MC19 and calcite rafts. Square brackets indicate activity ratios. Numbers in parentheses are 2σ uncertainties of the least significant digits.

Sample ID	Depth mm (±)	U $ng\,g^{-1}$	$[^{230}Th/^{232}Th]$	$[^{230}Th/^{238}U]$ (2σ)	$[^{234}U/^{238}U]_i$ (2σ)	$[^{232}Th/^{238}U]$ (2 SE)	Uncorr. age ka (2σ)	Corr. age ka (2σ)	$[^{234}U/^{238}U]_i$ corr. (2 SE)
Pendulite (stalactite interior)									
MC19-18		1258	299.5	1.2490(46)	1.1581(18)	0.004170(83)		No age	
MC19-13		267	891.5	1.2235(80)	1.1577(34)	0.001372(27)	705.05(264.54)	702(+inf/ − 149)	2.2823(2.7950)
MC19-19		299	3787.0	1.1922(69)	1.1448(31)	0.000315(06)	518.11(67.09)	513(+85/ − 50)	1.6275(1182)
MC19-15		573	146.5	1.3983(63)	1.4215(28)	0.009546(191)	258.24(4.47)	258.1(4.6)	1.8735(99)
MC19-14		434	1087.0	1.2691(64)	1.3219(29)	0.001167(23)	250.01(4.71)	250.0(4.7)	1.6518(79)
Pendulite (subaqueous portion)									
MC19-02	19.4(0.8)	2227	1963.5	1.8314(79)	3.6786(54)	0.000933(19)	68.48(0.40)	68.42(0.40)	4.2497(63)
MC19-03	18.1(1.0)	2086	2661.5	1.8988(86)	3.8646(59)	0.000713(14)	67.26(0.41)	67.19(0.41)	4.4633(69)
MC19-04	16.1(0.7)	2051	3266.4	1.8884(106)	3.9279(75)	0.000578(12)	65.39(0.49)	65.32(0.49)	4.5213(88)
MC19-05	13.1(0.9)	2003	1586.7	1.5104(88)	3.8244(70)	0.000952(19)	51.31(0.38)	51.23(0.38)	4.2645(79)
MC19-06	12.1(0.8)	1637	1527.6	1.4752(79)	3.8599(64)	0.000966(19)	49.31(0.33)	49.25(0.34)	4.2869(71)
MC19-07	9.9(0.5)	1513	3133.6	1.4774(92)	3.9537(76)	0.000471(09)	48.01(0.37)	47.94(0.37)	4.3822(84)
MC19-08	8.5(0.7)	1543	3334.6	1.4804(81)	3.9789(67)	0.000444(09)	47.75(0.32)	47.69(0.32)	4.4086(73)
MC19-09	5.5(0.7)	2226	1967.5	1.4073(72)	3.9613(61)	0.000715(14)	45.21(0.28)	45.14(0.28)	4.3643(67)
MC19-10	4.5(0.8)	1939	2568.1	1.3967(80)	3.9797(69)	0.000544(11)	44.57(0.31)	44.50(0.32)	4.3791(75)
MC19-11	3.2(0.9)	2242	593.3	1.3861(75)	4.0053(65)	0.002336(47)	43.77(0.31)	43.70(0.31)	4.4004(71)
MC19-12	2.1(0.8)	2026	750.6	1.3567(72)	4.0361(64)	0.001807(36)	42.32(0.28)	42.25(0.28)	4.4212(70)
MC19-17	1.0(0.4)	1406	151.4	0.6702(50)	4.0744(68)	0.004426(89)	19.00 (0.23)	18.94(0.23)	4.2438(72)
MC19-20	0.2(0.1)	1404	132.9	0.5846(34)	4.0693(53)	0.004398(88)	16.43(0.20)	16.36(0.20)	4.2149(57)
Dusty calcite raft									
MCCR-33_1		2842	6.2	0.0040(03)	4.0909(168)	0.000679(45)	0.080(28)	0.007(0.028)	4.0916(168)
MCCR-33_2		2949	10.8	0.0033(04)	4.0850(264)	0.000338(32)	0.075(17)	0.002(0.017)	4.0857(264)
MCCR-33_3		2809	11.4	0.0038(01)	4.0721(200)	0.000344(26)	0.088(14)	0.015(0.014)	4.0728(200)
MCCR-33_4		2694	12.8	0.0059(02)	4.0739(199)	0.000473(33)	0.139(20)	0.066(0.020)	4.0751(199)
Clean calcite rafts									
MCCR-10		2554	7.4	0.0031(03)	4.0746(79)	0.000432(12)	0.083(08)	−0.0179(0.0086)	4.0751(79)
MCCR-12		2514	11.0	0.0040(02)	4.0806(91)	0.000372(10)	0.107(05)	0.0100(0.0060)	4.0813(91)
MCCR-16		2584	9.9	0.0056(03)	4.0712(76)	0.000573(14)	0.150(08)	0.0402(0.0089)	4.0722(76)
MCCR-18		2698	12.1	0.0059(02)	4.0773(91)	0.000498(10)	0.158(05)	0.0528(0.0062)	4.0783(90)
MCCR-20		2509	15.3	0.0041(02)	4.0780(75)	0.000274(05)	0.110(05)	0.0191(0.0057)	4.0787(74)
MCCR-22		2835	8.2	0.0077(02)	4.0810(80)	0.000957(19)	0.206(05)	0.0713(0.0083)	4.0823(80)
MCCR-23		2230	3.0	0.0305(05)	4.0626(78)	0.010261(264)	0.821(14)	0.083(0.070)	4.0640(78)
MCCR-26		2410	10.0	0.0057(03)	4.0803(86)	0.000589(21)	0.152(08)	0.0415(0.0089)	4.0813(85)
MCCR-25		2561	9.5	0.0029(02)	4.0685(86)	0.000318(06)	0.078(05)	−0.0158(0.0058)	4.0690(87)
MCCR-29		2430	22.0	0.0396(05)	4.0633(70)	0.001806(30)	1.067(14)	0.877(0.018)	4.0715(70)
MCCR-30		4203	13.3	0.0026(02)	4.0772(83)	0.000205(04)	0.070(05)	−0.0166(0.0055)	4.0777(83)
MCCR-31		2552	9.5	0.0042(03)	4.0811(77)	0.000456(08)	0.112(08)	0.0099(0.0086)	4.0819(78)

Table 4. Radiocarbon dating results for the calcite rafts and calculated dead carbon fractions.

ANSTO code	Sample ID	$\delta^{13}C$ ‰	1σ	pMC	1σ	yr BP	1σ	yr BP (U–Th)	2σ	pMC_{atm}	1σ	DCF (%)	1σ
OZBK55	MCCR-30	−5.5	0.1	58.41	0.18	4319	25	−16.6	5.5				
OZBK53	MCCR-25	−6.2	0.3	57.50	0.19	4445	27	−15.8	5.8				
OZBK56	MCCR-31	−5.5	0.1	58.39	0.18	4322	25	9.9	8.6	98.05	0.44	40.45	0.33
OZBK54	MCCR-26	−5.5	0.3	57.72	0.17	4415	24	41.5	8.9	98.46	0.43	41.38	0.31

Table 5. Radiocarbon results for the groundwater.

ANSTO code	Sample ID	$\delta^{13}C$ ‰	1σ	pMC	1σ	Uncorr. yr BP	1σ	Total CO_2 (DIC mEq L^{-1})	Corr. yr BP
OZAS59	M1-C1	−12.9	0.6	49.92	0.14	5580	25	5.76	589

sions or impounded basins developed in the cave floor (e.g. Drysdale et al., 2019). However, this is only possible where the cave floor is impermeable. The Etina limestone and the neighbouring siltstone formations on either side are all near vertical (Fig. 2), with a consistent dip of $\sim 80°$ along the entire 10 km length of these outcrops. Therefore, it is unlikely that there is an aquitard below the cave that could allow water to pool to create a perched aquifer. Furthermore, an impossibly high discharge of vadose percolation water would be required to fill the volume of the main chamber to the observed level of the standing water mark, or the water level observed by cavers in 1974.

The calcite rafts and the subaqueous portion of the pendulite exhibit similar Mg / Ca and Sr / Ca values, which are 2–4 times higher than the values observed in the subaerial speleothems, i.e. the stalactite portion of the pendulite and the two stalagmites studied by Treble et al. (2017). This confirms that the subaqueous and the subaerial (drip-fed) calcites precipitated from different parent waters. Therefore, pooling dripwater is unlikely to be the parent water from which the subaqueous formations precipitated. Rising of the regional water table is thus the most likely mechanism to explain the flooding of Mairs Cave. The groundwater is supersaturated with respect to calcite ($SI_{cc} = 1.12$), meaning calcite will readily precipitate from the groundwater. The Mg / Ca and Sr / Ca values of the subaerial calcites fall outside of the ranges of values that could occur in calcites precipitated from the groundwater, whereas the Mg / Ca and Sr / Ca values of the subaqueous calcites fall within these ranges (see Fig. 6). These findings indicate that it is entirely possible for the subaqueous formations to have precipitated from the groundwater.

U–Th dating revealed markedly different initial uranium isotope ratios ($[^{234}U/^{238}U]_i$) between the subaerial calcite (1.56–2.95) and the subaqueous calcite (4.07–4.52). Alpha recoil during radioactive decay of ^{238}U in the bedrock causes ^{234}Th to be expelled across grain boundaries and into pore spaces, where it rapidly decays into ^{234}U and can be entrained by infiltrating water (Kigoshi, 1971; Osmond et al., 1992; Osmond and Cowart, 1976; Plater et al., 1992). ^{234}U can also diffuse into porewater via alpha recoil tracks. The longer infiltrating water spends in the bedrock, the more ^{234}U it will acquire. This would explain why the subaqueous calcite has higher $[^{234}U/^{238}U]_i$ than the calcite precipitated from dripwater, considering some studies have observed dripwater arriving in a cave in a matter of hours (Markowska et al., 2016), while the groundwater has a residence time of 661 years, according to the radiocarbon dating results. Therefore, the initial uranium isotope data also indicate rising groundwater is the mechanism responsible for flooding Mairs Cave.

Meteoric water that infiltrates the subsurface becomes slightly acidic by dissolution of CO_2 that is present in the soil due to microbial and root respiration (Fairchild and Baker, 2012). The $[^{14}C]$ of the soil CO_2 should be close to or at equilibrium with the atmosphere (Fohlmeister et al., 2011). When the water subsequently percolates through and dissolves carbonate bedrock, the $[^{14}C]$ of the DIC will be reduced because carbonate bedrocks, typically on the order of $10^5 - 10^8$ yr old, exhibit a $[^{14}C]$ equal to zero (Clark, 2015). The DCF is a term used to describe what portion of the carbon present in a sample was contributed by exchange with the bedrock or other "dead" carbon reservoirs. The groundwater in Buckalowie Valley returned a DCF of 45.8 %; meanwhile, the calcite rafts returned DCFs of 41.38 % and 40.45 %. Considering uncertainties inherit to radiocarbon corrections and the DCF variability observed in speleothems (Griffiths et al., 2012; Hua et al., 2012; Welte et al., 2021), the DCFs of the groundwater and the calcite rafts show remarkable similarity, which serves as additional evidence that flooding of the cave can be attributed to rising of the water table during periods of enhanced groundwater recharge.

5.2 The groundwater context

Assuming similarity to other groundwater systems in the Ikara-Flinders Ranges, the impermeable formations that comprise the valley walls most likely act as hydrological divides that constrain the extent of the aquifer (Ahmed et al., 2021; Ahmed and Clark, 2016; Fildes et al., 2020). However, given the high degree of fracturing caused by the orogenic history of the region, it is highly likely that the aquifer hosted in the limestone exhibits some hydrological connectivity to neighbouring groundwater systems. Nevertheless, the age (588.84 yr) and shallowness (5.54 m depth to water) of the groundwater in Buckalowie Valley are indicative of a localised and dynamic system that is unlikely to be mixing with a deeper and older regional aquifer.

The fact that the groundwater sample contains a portion of modern water (indicated by the presence of tritium) suggests that the bore and cave are within the recharge region of an active groundwater system, implying no significant lag between when meteoric waters first enter the subsurface and their arrival in the cave. For example, if Mairs Cave were to experience a prolonged rise in the water table to (re-)initiate subaqueous growth, the "age" of the infiltrating waters submerging the pendulites would likely be relatively young (10^0-10^1 yr) or at most contain a component of 10^2 yr old water. Thus, we interpret that millennial-scale climate events should be detectable in a proxy record from MC19, with a temporal offset of no more than 10^1-10^2 yr, assuming groundwater flow has not changed significantly since subaqueous pendulite growth began. Considering there does not appear to be any significant mixing with older groundwaters, proxy signals are unlikely to exhibit excessive temporal smoothing.

The groundwater context in which MC19 grew offers advantages over classical (vadose zone drip-fed) speleothems. Monitoring studies have shown that dripwater chemistry may be heterogenous between drip points, due to heterogeneity in flow paths and/or geochemical composition of the bedrock. The effects of these factors are often amplified in arid regions (Fairchild et al., 2006; McDonough et al., 2016) and can translate to coeval stalagmites returning dissimilar geochemical records from the same cave, raising the need for duplication of stalagmite records and/or interpretations that are supported by cave monitoring (Treble et al., 2022). In contrast, the proxy signals that MC19 inherits from the groundwater will be homogeneous on the local scale, and the rise and fall of the water table is more likely to be responsive to regional hydroclimate variability than to the nuances of a single drip path.

"Thorium scavenging" has been identified as a potential issue with the use of subaqueous speleothems for palaeoclimate reconstruction (Drysdale et al., 2019, 2020; Moseley et al., 2016). ^{230}Th present in the water due to the radioactive decay of dissolved uranium can be "scavenged" by speleothem calcite. The addition of non-authigenic ^{230}Th causes the calcite to appear older than it is. Where ^{230}Th concentration increases with depth, samples taken from deeper in the water column will appear systematically older than those taken from higher in the water column (Moseley et al., 2016). In a setting where water depth fluctuates over time, the speleothem will be exposed to variable ^{230}Th concentrations, resulting in age inversions. Despite fluctuating water levels in Mairs Cave, all ages taken from MC19 are in stratigraphic order, which suggests that thorium scavenging is unlikely to have altered the isotope activity ratios in the calcite.

5.3 Palaeoenvironmental interpretations

The calcite rafts in Mairs Cave are indisputable evidence that cave flooding has occurred, since they can only form at the surface of a body of water. The three youngest calcite rafts, dated to 1966 (±5.8 yr), 1967 (±5.5 yr), and 1968 (±8.6 yr), most likely correspond to the cave flooding event reported by cavers in 1968. Unfortunately, the age uncertainties are such that, beyond the historical record, the rafts cannot be used to confidently identify individual flooding events. While cave flooding during the last millennium was responsible for the precipitation of many calcite rafts, no appreciable amount of calcite was deposited on the surface of the pendulite. This suggests that cave flooding during the Holocene has been sporadic and ephemeral when compared to cave flooding during the LGP. Studies of groundwater systems in arid and semi-arid regions are increasingly showing that groundwater recharge occurs only when a site-specific infiltration threshold is exceeded by an extreme rainfall event (Boas and Mallants, 2022; Gelsinari et al., 2024; Jasechko, 2019; Jasechko and Taylor, 2015; Taylor et al., 2013; Villeneuve et al., 2015). At Mairs Cave, extreme rainfall events occur more often in summer than in any other season (BoM, 2024a). During summer, the subtropical ridge sits at $\sim 37°$ (Larsen and Nicholls, 2009), preventing rainfall coming off the Southern Ocean from reaching Mairs Cave (32° S); hence rainfall events during summer are primarily a consequence of the southward propagation of IASM depressions. Cave flooding in 1974 coincided with continent-wide rainfall extremes caused by an intensification and southward displacement of the IASM (Pook et al., 2014; BoM, 2024b).

Dates from the two most exterior laminae of MC19 returned ages of 16.4 (±0.20) and 18.9 (±0.23) ka (Fig. 7a). We judge these to be two distinct bursts of growth rather than a period of continuous growth because the two laminae are separated by a micritic/microsparitic layer. The combined growth span of stalagmites MCS1 and MCS2 is from 24–15 ka (Fig. 7a), but, as interpreted from the isotopic records, the period of highest recharge to the groundwater occurred between 18.9 and 15.8 ka (Treble et al., 2017), showing close alignment with the two youngest growth bursts in the pendulite. A minimum in δ^{18}O at 17.2 ± 0.08 ka was interpreted by Treble et al. (2017) as an intensification of the IASM triggered by Heinrich 1 (H1; 17.5–14.7 ka; El Bani Altuna et al.,

2024). The burst of subaqueous growth in MC19 at 16.4 (±0.2) ka may also correspond to this event. Intensification and southward migration of the IASM due to H1 is evident in marine sediment records from Indonesia (Ardi et al., 2020; Muller et al., 2012; Steinke et al., 2014) and in speleothem records from northern Australia (Denniston et al., 2013a–c) and Indonesia (Ayliffe et al., 2013). Climate model precipitation outputs for the semi-arid and arid regions of Australia demonstrate a period of positive moisture balance between 17.5 and 14.7 ka which is attributed to increased delivery of tropical rainfall (Cadd et al., 2024). Given the broader continental context, it is plausible that H1 could have been responsible for the pulse of pendulite growth in Mairs Cave at 16.4 (±0.20) ka via southward displacement and/or intensification of the IASM.

The two extended phases of subaqueous calcite deposition on MC19 reveal that, during the LGP, cave flooding and thus enhanced groundwater recharge occurred not just as sporadic and ephemeral bursts but were sustained over millennia. This is indicative of a much more positive water balance than in the present day. These findings support an emerging paradigm shift which suggests that, in an Australian context, moisture availability is elevated during glacials relative to interglacials (Weij et al., 2024). Flooding of Mairs Cave sustained over multi-millennial periods during the LGP could reflect more frequent southward incursions and/or increased intensity of the IASM, in conjunction with a reduced recharge threshold due to lower evapotranspiration. This interpretation is consistent with findings from the Naracoorte Cave Complex (600 km SSE of Mairs Cave), where speleothem growth under glacial climates has been linked to tropically sourced warm-season moisture (Weij et al., 2024).

The most recent multi-millennial growth period in MC19 occurred between 51.2 (±0.38) and 42.3 (±0.28; Fig. 7a) ka. We propose that this period of pendulite growth can also be attributed to the IASM, since (1) there is SH summer insolation maximum at 46 ka (Fig. 7b; Laskar et al., 2004); (2) the most recent period of interconnectivity between Kati Thanda and Munda occurred between 49.4 (±2.4) and 46.8 (±2.3) ka (Cohen et al., 2015); (3) high lake levels were sustained between ∼ 50 and 37 ka at Paruku / Gregory Lakes (20° S; Bowler et al., 2001; Fitzsimmons et al., 2012; Veth et al., 2009); (4) a highstand at Lake Woods (18° S) between 53 and 30 ka was proposed by Bowler et al. (1998); (5) neodymium isotope data from MD03-2607 (Fig. 7e) suggest an increase in outflow from the Darling River between 48 and 46 ka (Bayon et al., 2017); and, (6) from 60–40 ka, low percentages of subpolar and transitional foraminifera species in ocean core MD03-2611 (Fig. 7f; 36° S) would suggest that the subtropical and subpolar fronts were positioned further south relative to the present (De Deckker et al., 2020). Under these conditions, southern Australia would be unlikely to receive any significant amount of rainfall off the Southern Ocean, indicating that pendulite growth between 51.2 and 42.3 ka was most likely related to increased tropical moisture delivery.

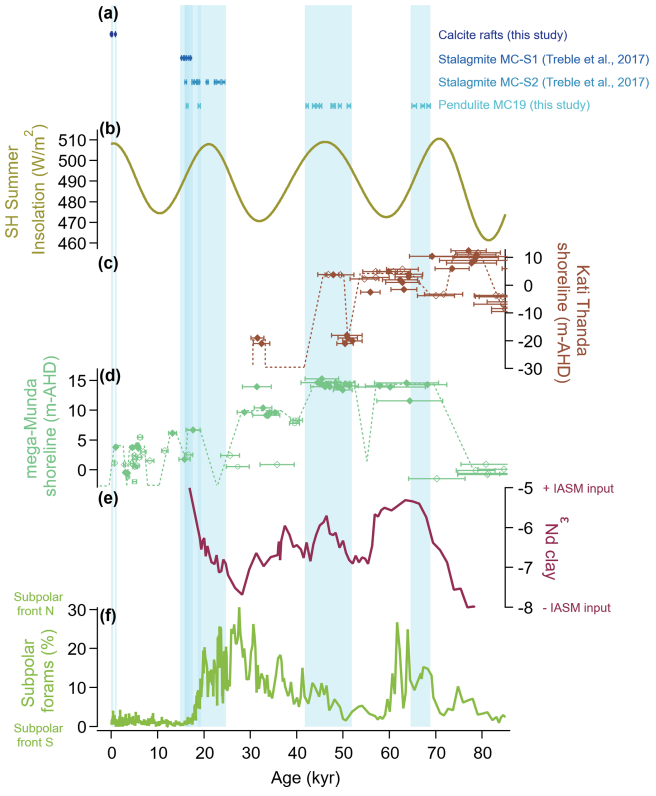

Figure 7. Shaded vertical bars indicate when Mairs Cave speleothems were growing. **(a)** Dates (including 2σ error bars) from Mairs Cave speleothems. **(b)** Summer insolation at 32.5° S from Laskar et al. (2004). **(c)** Height of shorelines at Kati Thanda / Lake Eyre. Filled diamonds are data from Magee et al. (2004). Unfilled diamonds are data from Cohen et al. (2015, 2022). **(d)** Height of shorelines at Munda / Lake Frome. Filled diamonds are from Cohen et al. (2011, 2012). Unfilled diamonds are from May et al. (2015). Unfilled circles are from Gliganic et al. (2014). **(e)** Neodymium isotopes ($^{\varepsilon}$Nd) in MD03-2607 representing relative sediment contributions from the Darling River (-2.4 ± 2.4) and the Murray River (-9.5 ± 0.9) from Bayon et al. (2017). An increase in contributions from the Darling River is considered indicative of an increase in the strength of the IASM. **(f)** Percentage of subpolar planktic foraminiferal species in core MD03-2611 for the Murray Canyon from De Deckker et al. (2020). An increase implies northward expansion of the subpolar and subtropical fronts, most likely accompanied by the SHWWs. Colours are assigned according to the recommendations of Crameri et al. (2020).

The cause of the older phase of pendulite growth (68.5–65.4 ka) is more difficult to designate. Regressional facies dated to 70.8 (±3.8) ka suggest a decline in Kati Thanda lake levels (Fig. 7c) that may have persisted until 60 (±2) ka (Cohen et al., 2022). This decline is not evident in Munda (Fig. 7d), where high lake levels were sustained between 68.2 (±4.2) and 60.1 (±7.6) ka (Cohen et al., 2015). A rapid and dramatic increase in the subpolar foraminifera species in MD03-2611 (Fig. 7f) between 70 and 60 ka suggests a northward displacement of the subpolar front (De Deckker et al.,

2020). Meanwhile, neodymium isotope data from MD03-2607 (Fig. 7e) suggest a southward shift in the IASM between 68 and 54 ka (Bayon et al., 2017), and there is an increase in speleothem growth at Naracoorte that appears closely coupled to the peak in local summer insolation between 75 and 65 ka (Weij et al., 2024). These contradictory results make it difficult to elucidate the behaviour of the IASM and the SHWWs throughout this period, and further interrogation of the pendulite record will be required to identify the cause of this growth phase.

6 Conclusion

Observations within the cave, along with historical archives and caving reports, suggest that Mairs Cave is periodically flooded. Speleothems hanging from the cave ceiling exhibit external and internal morphology typical of pendulites, which form when stalactites become submerged in water that is saturated with respect to calcium carbonate. Subsequent growth continues subaqueously whilst the pendulite is submerged but ceases when the water recedes. Mg / Ca and Sr / Ca ratios in the subaqueous calcite fall within the range of values that could theoretically occur in calcite precipitated from the measured groundwater. A saturation index of 1.12 suggests that calcite would be readily precipitated from the groundwater. There is remarkable agreement between the DCFs of the calcite rafts (41.38 % and 40.45 %) and the groundwater (45.8 %), and the subaqueous calcite exhibits much higher initial uranium isotope ratios than the subaerial calcites ($\mu = 4.00$ versus $\mu = 1.78$). These lines of evidence support the conclusion that rising of the water table during periods of enhanced groundwater recharge is the cause of cave flooding events. Consequently, we interpret that pendulite growth indicates periods when the water table was higher relative to the present.

The presence of tritium (0.13 TU) in the groundwater sample indicates that the bore and cave are within an active recharge region, and the ^{14}C age (589 yr BP) indicates negligible mixing with a deeper and older regional aquifer. Therefore, geochemical signals contained in the subaqueous speleothems are unlikely to exhibit smoothing or a temporal offset $\geq 10^2$ yr. Dating of the subaqueous pendulite material returned ages in stratigraphic order, so it appears unlikely that thorium scavenging occurred. We therefore conclude that the subaqueous pendulite growth may be ideal for further palaeoclimate investigations, as it is a record of past water table highstands, which are a function of groundwater recharge and hydroclimate variability.

Historical observations and the lack of pendulite growth indicate that strong water deficits under warm Holocene interglacial conditions give rise to episodic, rather than persistent, cave flooding. In contrast, during the LGP, the pendulite underwent two multi-millennial growth phases and two short bursts of growth. The youngest burst of growth (16.4 ka) may correspond to an intensification and southward displacement of the IASM triggered by H1. Comparison to other palaeoclimate records suggests that the longest of the two pendulite growth phases (51.2–42.3 ka) also occurred in response to enhanced tropical moisture delivery. Contradictory findings across other Australian records mean the older pendulite growth phase (68.5–65.4 ka) cannot yet be confidently attributed to the behaviour of either the IASM or the SHWWs.

While the cause of Australia's pluvial periods through the LGP will require further investigation, the pendulite from Mairs Cave offers a clear advantage over other archives from the arid zone; the timing of pluvial periods can be constrained with much greater precision. Situated on the southern boundary of Australia's arid zone, and at the interface between mid-latitudinal and tropical climate systems, Mairs Cave will undoubtedly provide much-needed insight into the climate of a region wanting in palaeoclimate records. Future studies will seek to reconstruct the climate of Australia's arid zone with greater temporal resolution using proxy records from multiple pendulites.

Data availability. The groundwater cation data are available in Table 1. Physical properties and major anions measured on the groundwater are available in Table 2. U-Th data are available in Table 3. The radiocarbon results for the calcite rafts are available in Table 4. The radiocarbon results for the groundwater are available in Table 5. Only average values from a large set of laser ablation ICPMS data are quoted in this study. They allow us to geochemically discriminate between subaqueous and subaerial calcite deposition. A detailed analysis of the full dataset is in progress, after which the data will be made available. Please contact the corresponding author for details.

Author contributions. CNGW, RND, PCT, and JHM designed the project and wrote the paper, with contributions from all authors. CNGW, RND, JCH, and CCB collected the calcite and groundwater samples. CNGW milled powdered samples, performed petrographic analysis, and prepared samples for U–Th dating. JCH performed U–Th dating. PCT calculated the calcite saturation index of the groundwater. SCP corrected the groundwater radiocarbon results and advised on the interpretation of all groundwater results. JHM advised on the comparison to regional palaeoenvironmental archives. CRV measured cation and anion concentrations in the groundwater samples. CCB sourced historical documents and caving records.

Competing interests. At least one of the (co-)authors is a member of the editorial board of *Climate of the Past*. The peer-review process was guided by an independent editor, and the authors also have no other competing interests to declare.

Disclaimer. Publisher's note: Copernicus Publications remains neutral with regard to jurisdictional claims made in the text, pub-

lished maps, institutional affiliations, or any other geographical representation in this paper. While Copernicus Publications makes every effort to include appropriate place names, the final responsibility lies with the authors.

Acknowledgements. We are grateful to Quan Hua for performing the radiocarbon analyses on the calcite samples and assisting in the interpretation of the results. We thank Alan Greig for performing the trace element analysis by LA-ICP mass spectrometry. We thank Henri Wong for assisting with trace element analyses of calcites and groundwater by ICP atomic emission spectroscopy and with anion measurements of groundwater by IC. We thank Silvia Frisia for her contributions to the classification of calcite fabrics.

Financial support. This project was funded by Australian Research Council Discovery Project grant no. DP220102134 (to Russell N. Drysdale, Pauline C. Treble, and John C. Hellstrom) and Herman Slade Foundation grant no. HSF21073 (to Russell N. Drysdale, Calla N. Gould-Whaley, and Clare C. Buswell). We acknowledge the support for the Centre for Accelerator Science at ANSTO through the Australian National Collaborative Research Infrastructure Strategy (NCRIS). Calla N. Gould-Whaley was the recipient of an Australian Institute of Nuclear Science and Engineering (AINSE) Post-Graduate Research Award (PGRA), which funded analyses performed at ANSTO.

Review statement. This paper was edited by Shiling Yang and reviewed by two anonymous referees.

References

Ahmed, A. and Clark, I.: Groundwater flow and geochemical evolution in the Central Flinders Ranges, South Australia, Sci. Total Environ., 572, 837–851, https://doi.org/10.1016/j.scitotenv.2016.07.123, 2016.

Ahmed, A., Alrajhi, A., and Alquwaizany, A. S.: Identification of Groundwater Potential Recharge Zones in Flinders Ranges, South Australia Using Remote Sensing, GIS, and MIF Techniques, Water (Basel), 13, 2571, https://doi.org/10.3390/w13182571, 2021.

Ardi, R. D. W., Aswan, Maryunani, K. A., Yulianto, E., Putra, P. S., Nugroho, S. H., and Istiana: Last deglaciation-holocene Australian-Indonesian monsoon rainfall changes off southwest Sumba, Indonesia, Atmosphere, 11, 932, https://doi.org/10.3390/atmos11090932, 2020.

Arora, V. K.: The use of the aridity index to assess climate change effect on annual runoff, J. Hydrol., 265, 164–177, https://doi.org/10.1016/S0022-1694(02)00101-4, 2002.

Atsawawaranunt, K., Comas-Bru, L., Amirnezhad Mozhdehi, S., Deininger, M., Harrison, S. P., Baker, A., Boyd, M., Kaushal, N., Ahmad, S. M., Ait Brahim, Y., Arienzo, M., Bajo, P., Braun, K., Burstyn, Y., Chawchai, S., Duan, W., Hatvani, I. G., Hu, J., Kern, Z., Labuhn, I., Lachniet, M., Lechleitner, F. A., Lorrey, A., Pérez-Mejías, C., Pickering, R., Scroxton, N., and SISAL Working Group Members: The SISAL database: a global resource to document oxygen and carbon isotope records from speleothems, Earth Syst. Sci. Data, 10, 1687–1713, https://doi.org/10.5194/essd-10-1687-2018, 2018.

Ayliffe, L. K., Gagan, M. K., Zhao, J. X., Drysdale, R. N., Hellstrom, J. C., Hantoro, W. S., Griffiths, M. L., Scott-Gagan, H., Pierre, E. S., Cowley, J. A., and Suwargadi, B. W.: Rapid interhemispheric climate links via the Australasian monsoon during the last deglaciation, Nat. Commun., 4, 1–6, https://doi.org/10.1038/ncomms3908, 2013.

Bajo, P., Hellstrom, J., Frisia, S., Drysdale, R., Black, J., Woodhead, J., Borsato, A., Zanchetta, G., Wallace, M. W., Regattieri, E., and Haese, R.: "Cryptic" diagenesis and its implications for speleothem geochronologies, Quaternary Sci. Rev., 148, 17–28, https://doi.org/10.1016/j.quascirev.2016.06.020, 2016.

El Bani Altuna, N., Ezat, M. M., Smik, L., Muschitiello, F., Belt, S. T., Knies, J., and Rasmussen, T. L.: Sea ice–ocean coupling during Heinrich Stadials in the Atlantic–Arctic gateway, Sci. Rep., 14, 1065, https://doi.org/10.1038/s41598-024-51532-7, 2024.

Bateman, M. D., Boulter, C. H., Carr, A. S., Frederick, C. D., Peter, D., and Wilder, M.: Preserving the palaeoenvironmental record in Drylands: Bioturbation and its significance for luminescence-derived chronologies, Sediment. Geol., 195, 5–19, https://doi.org/10.1016/j.sedgeo.2006.07.003, 2007.

Bayon, G., De Deckker, P., Magee, J. W., Germain, Y., Bermell, S., Tachikawa, K., and Norman, M. D.: Extensive wet episodes in Late Glacial Australia resulting from high-latitude forcings, Sci. Rep.-UK, 7, 1–7, https://doi.org/10.1038/srep44054, 2017.

Beck, H. E., Zimmermann, N. E., McVicar, T. R., Vergopolan, N., Berg, A., and Wood, E. F.: Present and future Köppen–Geiger climate classification maps at 1 km resolution, Sci. Data, 7, 274, https://doi.org/10.1038/s41597-020-00616-w, 2020.

Boas, T. and Mallants, D.: Episodic extreme rainfall events drive groundwater recharge in arid zone environments of central Australia, J. Hydrol. Reg. Stud., 40, 101005, https://doi.org/10.1016/j.ejrh.2022.101005, 2022.

BOM: Australian Government, Bureau of Meteorology, Climate Data Online, Daily Rainfall, Cradock (Yednalue), Product Code: IDCJAC0009, Reference: 118334562, 2024a.

BOM: Australian Government, Bureau of Meteorology, Recent and historical rainfall maps, Australian rainfall deciles, 1 January to 31 December 1974, Australian Gridded Climate Data, Product Code: IDCK200A00, 2024b.

Bowler, J. M., Duller, G., Perret, N., Prescott, J. R., and Wyrwoll, K. H.: Hydrological changes in monsoonal climates of the last glacial period stratigraphy and luminescence dating of Lake Woods, Palaeoclimates, 3., 179–207, 1998.

Bowler, J. M., Wyrwoll, K.-H., and Lu, Y.: Variations of the northwest Australian summer monsoon over the last 300 000 years: the paleohydrological record of the Gregory (Mulan) Lakes System, Quatern. Int., 63–80, 2001.

Burrell, A. L., Evans, J. P., and De Kauwe, M. G.: Anthropogenic climate change has driven over 5 million km^2 of drylands towards desertification, Nat. Commun., 11, 3853, https://doi.org/10.1038/s41467-020-17710-7, 2020.

Cadd, H., Petherick, L., Tyler, J., Herbert, A., Cohen, T. J., Sniderman, K., Barrows, T. T., Fulop, R. H., Knight, J., Kershaw, A. P., Colhoun, E. A., and Harris, M. R. P.: A continental perspective on the timing of environmental change during

the last glacial stage in Australia, Quaternary Res., 102, 5–23, https://doi.org/10.1017/qua.2021.16, 2021.

Cadd, H., Williams, A. N., Saktura, W. M., Cohen, T. J., Mooney, S. D., He, C., Otto-Bliesner, B., and Turney, C. S. M.: Last Glacial Maximum cooling induced positive moisture balance and maintained stable human populations in Australia, Commun. Earth Environ., 5, 52, https://doi.org/10.1038/s43247-024-01204-1, 2024.

Carilli, J. E., McGregor, H. V., Gaudry, J. J., Donner, S. D., Gagan, M. K., Stevenson, S., Wong, H., and Fink, D.: Equatorial Pacific coral geochemical records show recent weakening of the Walker Circulation, Paleoceanography, 29, 1031–1045, https://doi.org/10.1002/2014PA002683, 2014.

Carr, A. S., Bateman, M. D., and Holmes, P. J.: Developing a 150 ka luminescence chronology for the barrier dunes of the southern Cape, South Africa, Quat. Geochronol., 2, 110–116, https://doi.org/10.1016/j.quageo.2006.09.002, 2007.

Cheng, H., Edwards, R. L., Sinha, A., Spötl, C., Yi, L., Chen, S., Kelly, M., Kathayat, G., Wang, X., Li, X., Kong, X., Wang, Y., Ning, Y., and Zhang, H.: The Asian monsoon over the past 640 000 years and ice age terminations, Nature, 534, 640–646, https://doi.org/10.1038/nature18591, 2016.

Clark, I.: Groundwater Geochemistry and Isotopes, CRC Press, 456 pp., https://doi.org/10.1201/b18347, 2015.

Cohen, T. J., Nanson, G. C., Jansen, J. D., Jones, B. G., Jacobs, Z., Treble, P., Price, D. M., May, J. H., Smith, A. M., Ayliffe, L. K., and Hellstrom, J. C.: Continental aridification and the vanishing of Australia's megalakes, Geology, 39, 167–170, https://doi.org/10.1130/G31518.1, 2011.

Cohen, T. J., Nanson, G. C., Jansen, J. D., Jones, B. G., Jacobs, Z., Larsen, J. R., May, J. H., Treble, P., Price, D. M., and Smith, A. M.: Late Quaternary mega-lakes fed by the northern and southern river systems of central Australia: Varying moisture sources and increased continental aridity, Palaeogeogr. Palaeocl., 356–357, 89–108, https://doi.org/10.1016/j.palaeo.2011.06.023, 2012.

Cohen, T. J., Jansen, J. D., Gliganic, L. A., Larsen, J. R., Nanson, G. C., May, J. H., Jones, B. G., and Price, D. M.: Hydrological transformation coincided with megafaunal extinction in central Australia, Geology, 43, 195–198, https://doi.org/10.1130/G36346.1, 2015.

Cohen, T. J., Arnold, L. J., Gázquez, F., May, J. H., Marx, S. K., Jankowski, N. R., Chivas, A. R., Garćia, A., Cadd, H., Parker, A. G., Jansen, J. D., Fu, X., Waldmann, N., Nanson, G. C., Jones, B. G., and Gadd, P.: Late quaternary climate change in Australia's arid interior: Evidence from Kati Thanda – Lake Eyre, Quaternary Sci. Rev., 292, https://doi.org/10.1016/j.quascirev.2022.107635, 2022.

Comas-Bru, L., Rehfeld, K., Roesch, C., Amirnezhad-Mozhdehi, S., Harrison, S. P., Atsawawaranunt, K., Ahmad, S. M., Brahim, Y. A., Baker, A., Bosomworth, M., Breitenbach, S. F. M., Burstyn, Y., Columbu, A., Deininger, M., Demény, A., Dixon, B., Fohlmeister, J., Hatvani, I. G., Hu, J., Kaushal, N., Kern, Z., Labuhn, I., Lechleitner, F. A., Lorrey, A., Martrat, B., Novello, V. F., Oster, J., Pérez-Mejías, C., Scholz, D., Scroxton, N., Sinha, N., Ward, B. M., Warken, S., Zhang, H., and SISAL Working Group members: SISALv2: a comprehensive speleothem isotope database with multiple age–depth models, Earth Syst. Sci. Data, 12, 2579–2606, https://doi.org/10.5194/essd-12-2579-2020, 2020.

Corrick, E. C., Drysdale, R. N., Hellstrom, J. C., Capron, E., Rasmussen, S. O., Zhang, X., Fleitmann, D., Couchoud, I., and Wolff, E.: Synchronous timing of abrupt climate changes during the last glacial period, Science, 369, 963–969, https://doi.org/10.1126/science.aay5538, 2020.

Crameri, F., Shephard, G. E., and Heron, P. J.: The misuse of colour in science communication, Nat. Commun., 11, 5444, https://doi.org/10.1038/s41467-020-19160-7, 2020.

Cruz, F. W., Vuille, M., Burns, S. J., Wang, X., Cheng, H., Werner, M., Lawrence Edwards, R., Karmann, I., Auler, A. S., and Nguyen, H.: Orbitally driven east–west antiphasing of South American precipitation, Nat. Geosci., 2, 210–214, https://doi.org/10.1038/ngeo444, 2009.

Day, C. C. and Henderson, G. M.: Controls on trace-element partitioning in cave-analogue calcite, Geochim. Cosmochim. Ac., 120, 612–627, https://doi.org/10.1016/j.gca.2013.05.044, 2013.

De Deckker, P., Moros, M., Perner, K., Blanz, T., Wacker, L., Schneider, R., Barrows, T. T., O'Loingsigh, T., and Jansen, E.: Climatic evolution in the Australian region over the last 94 ka – spanning human occupancy –, and unveiling the Last Glacial Maximum, Quaternary Sci. Rev., 249, 106593, https://doi.org/10.1016/j.quascirev.2020.106593, 2020.

Denniston, R. F., Asmerom, Y., Lachniet, M., Polyak, V. J., Hope, P., An, N., Rodzinyak, K., and Humphreys, W. F.: A Last Glacial Maximum through middle Holocene stalagmite record of coastal Western Australia climate, Quaternary Sci. Rev., 77, 101–112, https://doi.org/10.1016/j.quascirev.2013.07.002, 2013a.

Denniston, R. F., Wyrwoll, K. H., Polyak, V. J., Brown, J. R., Asmerom, Y., Wanamaker, A. D., LaPointe, Z., Ellerbroek, R., Barthelmes, M., Cleary, D., Cugley, J., Woods, D., and Humphreys, W. F.: A Stalagmite record of Holocene Indonesian-Australian Summer Monsoon variability from the Australian tropics, Quaternary Sci. Rev., 78, 155–168, https://doi.org/10.1016/j.quascirev.2013.08.004, 2013b.

Denniston, R. F., Wyrwoll, K. H., Asmerom, Y., Polyak, V. J., Humphreys, W. F., Cugley, J., Woods, D., LaPointe, Z., Peota, J., and Greaves, E.: North Atlantic forcing of millennial-scale Indo-Australian monsoon dynamics during the Last Glacial period, Quaternary Sci. Rev., 72, 159–168, https://doi.org/10.1016/j.quascirev.2013.04.012, 2013c.

DeVogel, S. B., Magee, J. W., Manley, W. F., and Miller, G. H.: A GIS-based reconstruction of late Quaternary paleohydrology: Lake Eyre, arid central Australia, Palaeogeogr. Palaeocl., 204, 1–13, https://doi.org/10.1016/S0031-0182(03)00690-4, 2004.

Dey, R., Bador, M., Alexander, L. V., and Lewis, S. C.: The drivers of extreme rainfall event timing in Australia, Int. J. Climatol., 41, 6654–6673, https://doi.org/10.1002/joc.7218, 2021.

Drysdale, R. N., Paul, B. T., Hellstrom, J. C., Couchoud, I., Greig, A., Bajo, P., Zanchetta, G., Isola, I., Spötl, C., Baneschi, I., Regattieri, E., and Woodhead, J. D.: Precise microsampling of poorly laminated speleothems for U-series dating, Quat. Geochronol., 14, 38–47, https://doi.org/10.1016/j.quageo.2012.06.009, 2012.

Drysdale, R. N., Zanchetta, G., Baneschi, I., Guidi, M., Isola, I., Couchoud, I., Piccini, L., Greig, A., Wong, H., Woodhead, J. D., Regattieri, E., Corrick, E., Paul, B., Spötl, C., Denson, E., Gordon, J., Jaillet, S., Dux, F., and Hellstrom, J. C.: Par-

titioning of Mg, Sr, Ba and U into a subaqueous calcite speleothem, Geochim. Cosmochim. Ac., 264, 67–91, https://doi.org/10.1016/j.gca.2019.08.001, 2019.

Drysdale, R. N., Couchoud, I., Zanchetta, G., Isola, I., Regattieri, E., Hellstrom, J., Govin, A., Tzedakis, P. C., Ireland, T., Corrick, E., Greig, A., Wong, H., Piccini, L., Holden, P., and Woodhead, J.: Magnesium in subaqueous speleothems as a potential palaeotemperature proxy, Nat. Commun., 11, 5027, https://doi.org/10.1038/s41467-020-18083-7, 2020.

Fairchild, I. J. and Baker, A.: Speleothem Science: from process to past environments, Wiley-Blackwell, West Sussex, https://doi.org/10.1002/9781444361094, 2012.

Fairchild, I. J., Borsato, A., Tooth, A. F., Frisia, S., Hawkesworth, C. J., Huang, Y., McDermott, F., and Spiro, B.: Controls on trace element (Sr-Mg) compositions of carbonate cave waters: Implications for speleothem climatic records, Chem. Geol., 166, 255–269, https://doi.org/10.1016/S0009-2541(99)00216-8, 2000.

Fairchild, I. J., Smith, C. L., Baker, A., Fuller, L., Spötl, C., Mattey, D., and McDermott, F.: Modification and preservation of environmental signals in speleothems, Earth Sci. Rev., 75, 105–153, https://doi.org/10.1016/j.earscirev.2005.08.003, 2006.

Falster, G., Tyler, J., Grant, K., Tibby, J., Turney, C., Löhr, S., Jacobsen, G., Kershaw, A. P., and Stefan, L.: Millennial-scale variability in south-east Australian hydroclimate between 30 000 and 10 000 years ago, Quaternary Sci. Rev., 192, 106–122, https://doi.org/10.1016/j.quascirev.2018.05.031, 2018.

Faraji, M., Borsato, A., Frisia, S., Hartland, A., Hellstrom, J. C., and Greig, A.: High-resolution reconstruction of infiltration in the Southern Cook Islands based on trace elements in speleothems, Quaternary Res., 118, 20–40, https://doi.org/10.1017/qua.2023.51, 2024.

Feng, S. and Fu, Q.: Expansion of global drylands under a warming climate, Atmos. Chem. Phys., 13, 10081–10094, https://doi.org/10.5194/acp-13-10081-2013, 2013.

Field, E., Marx, S., Haig, J., May, J.-H., Jacobsen, G., Zawadzki, A., Child, D., Heijnis, H., Hotchkis, M., McGowan, H., and Moss, P.: Untangling geochronological complexity in organic spring deposits using multiple dating methods, Quat. Geochronol., 43, 50–71, https://doi.org/10.1016/j.quageo.2017.10.002, 2018.

Field, M. S., Kraemer, S. R., and Palmer, A. N.: A Lexicon of Cave and Karst Terminology with Special Reference to Environmental Karst Hydrology, United States Environmental Protection Agency, National Centre for Environmental Assessment, Office of Research and Development, EPA/600/R-02/003, Washington, 2002.

Fildes, S. G., Clark, I. F., Somaratne, N. M., and Ashman, G.: Mapping groundwater potential zones using remote sensing and geographical information systems in a fractured rock setting, Southern Flinders Ranges, South Australia, J. Earth Syst. Sci., 129, 160, https://doi.org/10.1007/s12040-020-01420-1, 2020.

Fitzsimmons, K. E., Miller, G. H., Spooner, N. A., and Magee, J. W.: Aridity in the monsoon zone as indicated by desert dune formation in the Gregory lakes basin, northwestern Australia, Aust. J. Earth Sci., 59, 469–478, https://doi.org/10.1080/08120099.2012.686171, 2012.

Fitzsimmons, K. E., Cohen, T. J., Hesse, P. P., Jansen, J., Nanson, G. C., May, J. H., Barrows, T. T., Haberlah, D., Hilgers, A., Kelly, T., Larsen, J., Lomax, J., and Treble, P.: Late Quaternary palaeoenvironmental change in the Australian drylands, Quaternary Sci. Rev., 74, 78–96, https://doi.org/10.1016/j.quascirev.2012.09.007, 2013.

Fohlmeister, J., Scholz, D., Kromer, B., and Mangini, A.: Modelling carbon isotopes of carbonates in cave drip water, Geochim. Cosmochim. Ac., 75, 5219–5228, https://doi.org/10.1016/j.gca.2011.06.023, 2011.

Ford, D. and Williams, P.: Speleogenesis: The Development of Cave Systems, in: Karst Hydrogeology and Geomorphology, Wiley, https://doi.org/10.1002/9781118684986.ch7, 2013.

Frisia, S.: Microstratigraphic logging of calcite fabrics in speleothems as tool for palaeoclimate studies, Int. J. Speleol., 44, 1–16, https://doi.org/10.5038/1827-806X.44.1.1, 2015.

Fromhold, T. A. and Wallace, M. W.: Regional recognition of the Neoproterozoic Sturtian–Marinoan boundary, Northern and Central Adelaide Geosyncline, South Australia, Aust. J. Earth Sci., 59, 527–546, https://doi.org/10.1080/08120099.2012.673507, 2012.

Fu, X., Cohen, T. J., and Arnold, L. J.: Extending the record of lacustrine phases beyond the last interglacial for Lake Eyre in central Australia using luminescence dating, Quaternary Sci. Rev., 162, 88–110, https://doi.org/10.1016/j.quascirev.2017.03.002, 2017.

Fujioka, T. and Chappell, J.: History of Australian aridity: chronology in the evolution of arid landscapes, Geological Society, London, Special Publications, 346, 121–139, https://doi.org/10.1144/SP346.8, 2010.

Gelsinari, S., Bourke, S., McCallum, J., McFarlane, D., Hall, J., Silberstein, R., and Thompson, S.: Nonstationary recharge responses to a drying climate in the Gnangara Groundwater System, Western Australia, J. Hydrol., 633, 131007, https://doi.org/10.1016/j.jhydrol.2024.131007, 2024.

Giddings, J. A., Wallace, M. W., and Woon, E. M. S.: Interglacial carbonates of the Cryogenian Umberatana Group, northern Flinders Ranges, South Australia, Aust. J. Earth Sci., 56, 907–925, https://doi.org/10.1080/08120090903005378, 2009.

Gillieson, D.: Glossary of Cave and Karst Terminology, Wiley, 302–314, https://doi.org/10.1002/9781444313680.gloss, 1996.

Gliganic, L. A., Cohen, T. J., May, J. H., Jansen, J. D., Nanson, G. C., Dosseto, A., Larsen, J. R., and Aubert, M.: Late-Holocene climatic variability indicated by three natural archives in arid southern Australia, Holocene, 24, 104–117, https://doi.org/10.1177/0959683613515732, 2014.

Griffiths, M. L., Fohlmeister, J., Drysdale, R. N., Hua, Q., Johnson, K. R., Hellstrom, J. C., Gagan, M. K., and Zhao, J. x.: Hydrological control of the dead carbon fraction in a Holocene tropical speleothem, Quat. Geochronol., 14, 81–93, https://doi.org/10.1016/j.quageo.2012.04.001, 2012.

Grimes, K. G.: The Gregory Karst, Australian Speleological Federation, 2006.

Habeck-Fardy, A. and Nanson, G. C.: Environmental character and history of the Lake Eyre Basin, one seventh of the Australian continent, Earth Sci. Rev., 132, 39–66, https://doi.org/10.1016/j.earscirev.2014.02.003, 2014.

Han, L. F. and Plummer, L. N.: Revision of Fontes and Garnier's model for the initial ^{14}C content of dissolved inorganic carbon used in groundwater dating, Chem. Geol., 351, 105–114, https://doi.org/10.1016/j.chemgeo.2013.05.011, 2013.

Harrington, N. and Cook, P.: Groundwater in Australia, National Centre for Groundwater Research and Training, Flinders University, Adelaide, 2014.

Hellstrom, J.: Rapid and accurate U/Th dating using parallel ion-counting multi-collector ICP-MS, J. Anal. At. Spectrom., 18, 1346–1351, https://doi.org/10.1039/b308781f, 2003.

Hellstrom, J.: U-Th dating of speleothems with high initial 230Th using stratigraphical constraint, Quat. Geochronol., 1, 289–295, https://doi.org/10.1016/j.quageo.2007.01.004, 2006.

Hodge, E. J., Richards, D. A., Smart, P. L., Andreo, B., Hoffmann, D. L., Mattey, D. P., and González-Ramón, A.: Effective precipitation in southern Spain ($\sim$ 266 to 46 ka) based on a speleothem stable carbon isotope record, Quaternary Res. 69, 447–457, https://doi.org/10.1016/j.yqres.2008.02.013, 2008.

Hogg, A. G., Heaton, T. J., Hua, Q., Palmer, J. G., Turney, C. S., Southon, J., Bayliss, A., Blackwell, P. G., Boswijk, G., Bronk Ramsey, C., Pearson, C., Petchey, F., Reimer, P., Reimer, R., and Wacker, L.: SHCal20 Southern Hemisphere Calibration, 0–55 000 Years cal BP, Radiocarbon, 62, 759–778, https://doi.org/10.1017/RDC.2020.59, 2020.

Hua, Q., Jacobsen, G. E., Zoppi, U., Lawson, E. M., Williams, A. A., Smith, A. M., and McGann, M. J.: Progress in Radiocarbon Target Preparation at the Antares AMS Centre, Radiocarbon, 43, 275–282, https://doi.org/10.1017/S003382220003811X, 2001.

Hua, Q., McDonald, J., Redwood, D., Drysdale, R., Lee, S., Fallon, S., and Hellstrom, J.: Robust chronological reconstruction for young speleothems using radiocarbon, Quat. Geochronol., 14, 67–80, https://doi.org/10.1016/j.quageo.2012.04.017, 2012.

Huang, Y. and Fairchild, I. J.: Partitioning of Sr^{2+} and Mg^{2+} into calcite under karst-analogue experimental conditions, Geochim. Cosmochim. Ac., 65, 47–62, https://doi.org/10.1016/S0016-7037(00)00513-5, 2001.

Huang, Y., Fairchild, I. J., Borsato, A., Frisia, S., Cassidy, N. J., McDermott, F., and Hawkesworth, C. J.: Seasonal variations in Sr, Mg and P in modern speleothems (Grotta di Ernesto, Italy), Chem. Geol., 175, 429–448, https://doi.org/10.1016/S0009-2541(00)00337-5, 2001.

Jasechko, S.: Global Isotope Hydrogeology – Review, Rev. Geophys., 57, 835–965, https://doi.org/10.1029/2018RG000627, 2019.

Jasechko, S. and Taylor, R. G.: Intensive rainfall recharges tropical groundwaters, Environ. Res. Lett., 10, 124015, https://doi.org/10.1088/1748-9326/10/12/124015, 2015.

Jennings, J. N.: The Australian Speleological Quarterly: Cave and Karst Terminology, Broadway, 1979.

Jochum, K. P., Weis, U., Stoll, B., Kuzmin, D., Yang, Q., Raczek, I., Jacob, D. E., Stracke, A., Birbaum, K., Frick, D. A., Günther, D., and Enzweiler, J.: Determination of Reference Values for NIST SRM 610–617 Glasses Following ISO Guidelines, Geostand. Geoanal. Res., 35, 397–429, https://doi.org/10.1111/j.1751-908X.2011.00120.x, 2011.

Kalin, R. M.: Radiocarbon Dating of Groundwater Systems, in: Environmental Tracers in Subsurface Hydrology, Springer, Boston, https://doi.org/10.1007/978-1-4615-4557-6_4, 2000.

Kigoshi, K.: Alpha-Recoil Thorium-234: Dissolution into Water and the Uranium-234/Uranium-238 Disequilibrium in Nature, Science, 173, 47–48, https://doi.org/10.1126/science.173.3991.47, 1971.

Larsen, S. H. and Nicholls, N.: Southern Australian rainfall and the subtropical ridge: Variations, interrelationships, and trends, Geophys. Res. Lett., 36, https://doi.org/10.1029/2009GL037786, 2009.

Laskar, J., Robutel, P., Joutel, F., Gastineau, M., Correia, A. C. M., and Levrard, B.: A long-term numerical solution for the insolation quantities of the Earth, Astron. Astrophys., 428, 261–285, https://doi.org/10.1051/0004-6361:20041335, 2004.

Lawrence, R. E.: The Geological Context of Caves in the Flinders Ranges, South Australian Geographical Journal, 108, 59–78, 2009.

LeGrand, H. E.: Perspective on karst hydrology, J. Hydrol., 61, 343–355, https://doi.org/10.1016/0022-1694(83)90257-3, 1983.

LeGrand, H. E. and Stringfield, V. T.: Development and Distribution of Permeability in Carbonate Aquifers, Water Resour. Res., 7, 1284–1294, https://doi.org/10.1029/WR007i005p01284, 1971.

Leon, J. X. and Cohen, T. J.: An improved bathymetric model for the modern and palaeo Lake Eyre, Geomorphology, 173–174, 69–79, https://doi.org/10.1016/j.geomorph.2012.05.029, 2012.

Lu, J., Zhang, H., Li, H., Sha, L., Zhao, J., Li, Y., Wang, J., Dong, X., Edwards, R. L., Qian, Z., and Cheng, H.: A 120 year seasonally resolved speleothem record of precipitation seasonality from southeastern China, Quaternary Sci. Rev., 264, 107023, https://doi.org/10.1016/j.quascirev.2021.107023, 2021.

Magee, J. W., Bowler, J. M., Miller, G. H., and Williams, D. L. G.: Stratigraphy, sedimentology, chronology and palaeohydrology of Quaternary lacustrine deposits at Madigan Gulf, Lake Eyre, south Australia, Palaeogeogr. Palaeocl., 113, 3–42, https://doi.org/10.1016/0031-0182(95)00060-Y, 1995.

Magee, J. W., Miller, G. H., Spooner, N. A., and Questiaux, D.: Continuous 150 k.y. monsoon record from Lake Eyre, Australia: Insolation-forcing implications and unexpected Holocene failure, Geology, 32, 885–888, https://doi.org/10.1130/G20672.1, 2004.

Markowska, M., Baker, A., Andersen, M. S., Jex, C. N., Cuthbert, M. O., Rau, G. C., Graham, P. W., Rutlidge, H., Marjethoz, G., Marjo, C. E., Treble, P. C., and Edwards, N.: Semi-arid zone caves: Evaporation and hydrological controls on $\delta^{18}O$ drip water composition and implications for speleothem paleoclimate reconstructions, Quaternary Sci. Rev., 131, 285–301, https://doi.org/10.1016/j.quascirev.2015.10.024, 2016.

Markowska, M., Cuthbert, M. O., Baker, A., Treble, P. C., Andersen, M. S., Adler, L., Griffiths, A., and Frisia, S.: Modern speleothem oxygen isotope hydroclimate records in water-limited SE Australia, Geochim. Cosmochim. Ac., 270, 431–448, https://doi.org/10.1016/j.gca.2019.12.007, 2020.

Martín-García, R., Alonso-Zarza, A. M., Martín-Pérez, A., Schröder-Ritzrau, A., and Ludwig, T.: Relationships between colour and diagenesis in the aragonite-calcite speleothems in Basajaún Etxea cave, Spain, Sediment. Geol., 312, 63–75, https://doi.org/10.1016/j.sedgeo.2014.08.001, 2014.

Martínez-Aguirre, A., Alcaraz-Pelegrina, J. M., and Rodríguez-Vidal, J.: U/Th dating of impure carbonates: $^{230}Th/^{232}Th$ activity ratios in detrital material, J. Radioanal. Nucl. Ch., 321, 71–81, https://doi.org/10.1007/s10967-019-06560-3, 2019.

Martini, J. E. J. and Grimes, K. G.: Epikarstic Maze Cave Development: Bullita Cave System, Judbarra/Gregory Karst, Tropical Australia, Helectite, 37–66, 2012.

Mattey, D., Lowry, D., Duffet, J., Fisher, R., Hodge, E., and Frisia, S.: A 53 year seasonally resolved oxygen and carbon isotope record from a modern Gibraltar speleothem: Reconstructed drip water and relationship to local precipitation, Earth Planet. Sc. Lett., 269, 80–95, https://doi.org/10.1016/j.epsl.2008.01.051, 2008.

May, J. H., Barrett, A., Cohen, T. J., Jones, B. G., Price, D., and Gliganic, L. A.: Late Quaternary evolution of a playa margin at Lake Frome, South Australia, J. Arid Environ., 122, 93–108, https://doi.org/10.1016/j.jaridenv.2015.06.012, 2015.

May, J. H., May, S. M., Marx, S. K., Cohen, T. J., Schuster, M., and Sims, A.: Towards understanding desert shorelines – coastal landforms and dynamics around ephemeral Lake Eyre North, South Australia, T. Roy. Soc. South Aust., 146, 59–89, https://doi.org/10.1080/03721426.2022.2050506, 2022.

McDonough, L. K., Iverach, C. P., Beckmann, S., Manefield, M., Rau, G. C., Baker, A., and Kelly, B. F. J.: Spatial variability of cave-air carbon dioxide and methane concentrations and isotopic compositions in a semi-arid karst environment, Environ. Earth Sci., 75, 700, https://doi.org/10.1007/s12665-016-5497-5, 2016.

Meneghini, B., Simmonds, I., and Smith, I. N.: Association between Australian rainfall and the Southern Annular Mode, Int. J. Climatol., 27, 109–121, https://doi.org/10.1002/joc.1370, 2007.

Morgenstern, U. and Taylor, C. B.: Ultra low-level tritium measurement using electrolytic enrichment and LSC, Isot. Environ. Healt. S., 45, 96–117, https://doi.org/10.1080/10256010902931194, 2009.

Moseley, G. E., Edwards, R. L., Wendt, K. A., Cheng, H., Dublyansky, Y., Lu, Y., Boch, R., and Spötl, C.: Reconciliation of the Devils Hole climate record with orbital forcing, Science, 351, 165–168, https://doi.org/10.1126/science.aad4132, 2016.

Muller, J., McManus, J. F., Oppo, D. W., and Francois, R.: Strengthening of the Northeast Monsoon over the Flores Sea, Indonesia, at the time of Heinrich event 1, Geology, 40, 635–638, https://doi.org/10.1130/G32878.1, 2012.

Nanson, G. C., Callen, R. A., and Price, D. M.: Hydroclimatic interpretation of Quaternary shorelines on South Australian playas, Palaeogeogr. Palaeocl., 144, 281–305, https://doi.org/10.1016/S0031-0182(98)00123-0, 1998.

Osmond, J. K. and Cowart, J. B.: The theory and uses of natural uranium isotopic variations in hydrology, At Energy Rev., 14, 621–679, 1976.

Osmond, J. K., Ivanovich, M., and Harmon, R. S.: Mobilisation and weathering of U/Th series radionuclides, in: Uranium Series Disequilibrium: Application to Earth, Marine and Environmental Sciences, Clarenson Press, ISBN 0 19 854278 X, 1992.

Parkhurst, D. L. and Appelo, C. A. J.: User's guide to PHREEQC (Version 2): A computer program for speciation, batch-reaction, one-dimensional transport, and inverse geochemical calculations, https://doi.org/10.3133/wri994259, 1999.

Plater, A. J., Ivanovich, M., and Dugdale, R. E.: Uranium series disequilibrium in river sediments and waters: the significance of anomalous activity ratios, Appl. Geochem., 7, 101–110, https://doi.org/10.1016/0883-2927(92)90029-3, 1992.

Plummer, L. N. and Glynn, P. D.: Radiocarbon dating in groundwater systems, in: Isotope methods for dating old groundwater, IAEA, 33–89, 2013.

Pook, M. J., Risbey, J. S., Ummenhofer, C. C., Briggs, P. R., and Cohen, T. J.: A synoptic climatology of heavy rain events in the Lake Eyre and Lake Frome catchments, Front. Environ. Sci., 2, https://doi.org/10.3389/fenvs.2014.00054, 2014.

Sexton, R. T., Mullan, D., Kapelle, K., Mollet, N., and Hill, A. L.: Mairs Cave, Buckalowie Ck., Cave Exploration Group of South Australia, 1958.

Van Rampelbergh, M., Verheyden, S., Allan, M., Quinif, Y., Cheng, H., Edwards, L. R., Keppens, E., and Claeys, P.: A 500 year seasonally resolved $\delta^{18}O$ and $\delta^{13}C$, layer thickness and calcite aspect record from a speleothem deposited in the Han-sur-Lesse cave, Belgium, Clim. Past, 11, 789–802, https://doi.org/10.5194/cp-11-789-2015, 2015.

Reeves, J. M., Barrows, T. T., Cohen, T. J., Kiem, A. S., Bostock, H. C., Fitzsimmons, K. E., Jansen, J. D., Kemp, J., Krause, C., Petherick, L., Phipps, S. J., Armand, L. K., Ayliffe, L. K., Curran, M., De Deckker, P., Devriendt, L. S., Dodson, J., Dosseto, A., Dunbar, G. B., Drysdale, R. N., Fink, D., Fischer, M., Fletcher, M. S., Fujioka, T., Gagan, M. K., Griffiths, M. L., Haberlah, D., Haberle, S. G., Heikkila, U., Heijnis, H., Hesse, P. P., Hilgers, A., Ho, M., Howard, W., Hua, Q., Kelly, T., Larsen, J., Lewis, S., Lomax, J., Mackintosh, A., May, J. H., McGregor, H. V., Meisner, K., Mooney, S. D., Moss, P. T., Nanson, G. C., Pedro, J., Purcell, A., Shulmeister, J., Sloss, C., Swander, Z., Tibby, J., Treble, P., Van Der Kaars, S., White, D., and Woodward, C.: Climate variability over the last 35 000 years recorded in marine and terrestrial archives in the Australian region: An OZ-INTIMATE compilation, Quaternary Sci. Rev., 74, 21–34, https://doi.org/10.1016/j.quascirev.2013.01.001, 2013a.

Reeves, J. M., Bostock, H. C., Ayliffe, L. K., Barrows, T. T., De Deckker, P., Devriendt, L. S., Dunbar, G. B., Drysdale, R. N., Fitzsimmons, K. E., Gagan, M. K., Griffiths, M. L., Haberle, S. G., Jansen, J. D., Krause, C., Lewis, S., McGregor, H. V., Mooney, S. D., Moss, P., Nanson, G. C., Purcell, A., and van der Kaars, S.: Palaeoenvironmental change in tropical Australasia over the last 30 000 years – a synthesis by the OZ-INTIMATE group, Quaternary Sci. Rev., 74, 97–114, https://doi.org/10.1016/j.quascirev.2012.11.027, 2013b.

Reid, K. J., King, A. D., Lane, T. P., and Short, E.: The Sensitivity of Atmospheric River Identification to Integrated Water Vapor Transport Threshold, Resolution, and Regridding Method, J. Geophys. Res.-Atmos., 125, e2020JD032897, https://doi.org/10.1029/2020JD032897, 2020.

Scott, L.: Fluctuations of vegetation and climate over the last 75 000 years in the Savanna Biome, South Africa: Tswaing Crater and Wonderkrater pollen sequences reviewed, Quaternary Sci. Rev., 145, 117–133, https://doi.org/10.1016/j.quascirev.2016.05.035, 2016.

Skinner, L.: Facing future climate change: Is the past relevant?, Philos. T. R. Soc. A, 366, 4627–4645, https://doi.org/10.1098/rsta.2008.0228, 2008.

Steinke, S., Mohtadi, M., Prange, M., Varma, V., Pittauerova, D., and Fischer, H. W.: Mid- to Late-Holocene Australian-Indonesian summer monsoon variability, Quaternary Sci. Rev., 93, 142–154, https://doi.org/10.1016/j.quascirev.2014.04.006, 2014.

Stuiver, M. and Polach, H. A.: Discussion reporting of ^{14}C data, Radiocarbon, 19, 355–363, https://doi.org/10.1017/S0033822200003672, 1977.

Taylor, R. G., Todd, M. C., Kongola, L., Maurice, L., Nahozya, E., Sanga, H., and MacDonald, A. M.: Evidence of the dependence of groundwater resources on extreme rainfall in East Africa, Nat. Clim. Change, 3, 374–378, https://doi.org/10.1038/nclimate1731, 2013.

Telfer, M. W., Hesse, P. P., Perez-Fernandez, M., Bailey, R. M., Bajkan, S., and Lancaster, N.: Morphodynamics, boundary conditions and pattern evolution within a vegetated linear dunefield, Geomorphology, 290, 85–100, https://doi.org/10.1016/j.geomorph.2017.03.024, 2017.

Thomas, D. S. G. and Burrough, S. L.: Luminescence-based dune chronologies in southern Africa: Analysis and interpretation of dune database records across the subcontinent, Quatern. Int., 410, 30–45, https://doi.org/10.1016/j.quaint.2013.09.008, 2016.

Treble, P. C., Baker, A., Ayliffe, L. K., Cohen, T. J., Hellstrom, J. C., Gagan, M. K., Frisia, S., Drysdale, R. N., Griffiths, A. D., and Borsato, A.: Hydroclimate of the Last Glacial Maximum and deglaciation in southern Australia's arid margin interpreted from speleothem records (23–15 ka), Clim. Past, 13, 667–687, https://doi.org/10.5194/cp-13-667-2017, 2017.

Treble, P. C., Baker, A., Abram, N. J., Hellstrom, J. C., Crawford, J., Gagan, M. K., Borsato, A., Griffiths, A. D., Bajo, P., Markowska, M., Priestley, S. C., Hankin, S., and Paterson, D.: Ubiquitous karst hydrological control on speleothem oxygen isotope variability in a global study, Commun. Earth Environ., 3, 29, https://doi.org/10.1038/s43247-022-00347-3, 2022.

Tremaine, D. M. and Froelich, P. N.: Speleothem trace element signatures: A hydrologic geochemical study of modern cave dripwaters and farmed calcite, Geochim. Cosmochim. Ac., 121, 522–545, https://doi.org/10.1016/j.gca.2013.07.026, 2013.

Ünal-Imer, E., Shulmeister, J., Zhao, J. X., Uysal, I. T., and Feng, Y. X.: High-resolution trace element and stable/radiogenic isotope profiles of late Pleistocene to Holocene speleothems from Dim Cave, SW Turkey, Palaeogeogr. Palaeocl., 452, 68–79, https://doi.org/10.1016/j.palaeo.2016.04.015, 2016.

Vaks, A., Gutareva, O. S., Breitenbach, S. F. M., Avirmed, E., Mason, A. J., Thomas, A. L., Osinzev, A. V., Kononov, A. M., and Henderson, G. M.: Speleothems Reveal 500 000-Year History of Siberian Permafrost, Science, 340, 183–186, https://doi.org/10.1126/science.1228729, 2013.

Veth, P., Smith, M., Bowler, J., Fitzsimmons, K., Williams, A., and Hiscock, P.: Excavations At Parnkupirti, Lake Gregory, Great Sandy Desert: OSL Ages for Occupation before the Last Glacial Maximum, Aust. Archaeol., 69, 1–10, https://doi.org/10.1080/03122417.2009.11681896, 2009.

Villeneuve, S., Cook, P. G., Shanafield, M., Wood, C., and White, N.: Groundwater recharge via infiltration through an ephemeral riverbed, central Australia, J. Arid Environ., 117, 47–58, https://doi.org/10.1016/j.jaridenv.2015.02.009, 2015.

Wang, Y., Cheng, H., Edwards, R. L., Kong, X., Shao, X., Chen, S., Wu, J., Jiang, X., Wang, X., and An, Z.: Millennial- and orbital-scale changes in the East Asian monsoon over the past 224 000 years, Nature, 451, 1090–1093, https://doi.org/10.1038/nature06692, 2008.

Weij, R., Sniderman, J. M. K., Woodhead, J. D., Hellstrom, J. C., Brown, J. R., Drysdale, R. N., Reed, E., Bourne, S., and Gordon, J.: Elevated Southern Hemisphere moisture availability during glacial periods, Nature, 626, 319–326, https://doi.org/10.1038/s41586-023-06989-3, 2024.

Welte, C., Fohlmeister, J., Wertnik, M., Wacker, L., Hattendorf, B., Eglinton, T. I., and Spötl, C.: Climatic variations during the Holocene inferred from radiocarbon and stable carbon isotopes in speleothems from a high-alpine cave, Clim. Past, 17, 2165–2177, https://doi.org/10.5194/cp-17-2165-2021, 2021.

Wilcken, K. M., Hotchkis, M., Levchenko, V., Fink, D., Hauser, T., and Kitchen, R.: From carbon to actinides: A new universal 1 MV accelerator mass spectrometer at ANSTO, Nucl. Instrum. Meth. B, 361, 133–138, https://doi.org/10.1016/j.nimb.2015.04.054, 2015.

Williams, M., Cook, E., van der Kaars, S., Barrows, T., Shulmeister, J., and Kershaw, P.: Glacial and deglacial climatic patterns in Australia and surrounding regions from 35 000–10 000 years ago reconstructed from terrestrial and near-shore proxy data, Quaternary Sci. Rev., 28, 2398–2419, https://doi.org/10.1016/j.quascirev.2009.04.020, 2009.

Winton, L. J.: Report on the Mount Burr phosphate and guano mine, Mining Review, 32, 56–59, 1920.

Winton, L. J.: Report on the guano deposits held by Nitrogen Limited at Arcoota and Buckalowie Creeks. Counties Hanson and Granville, out of hundreds, Mining Review, 36, 57–61, 1922.

Zomer, R. J., Xu, J., and Trabucco, A.: Version 3 of the Global Aridity Index and Potential Evapotranspiration Database, Sci Data, 9, 409, https://doi.org/10.1038/s41597-022-01493-1, 2022.